

國立清華大學
電機資訊學院
光電工程研究所
碩士論文

超連續光譜壓縮至數週期短脈衝

**Few-Cycle Pulse Compression from
Supercontinuum**

研究生：陳柏翰

Student : Bo Han Chen

指導教授：孔慶昌 博士

Adviser : Andrew H. Kung

中華民國一百零四年七月

ACKNOWLEDGEMENT

I have been learning and working in this group for about three years. I met a lot of people here and got a lot of help from them. Without them, I won't finish my master's degree.

First, without a doubt, I want to thank my advisor, Andy Kung for teaching me and giving me advices during these three years. He is always enthusiastic about researches, and he can always come up with new ideas for experiments. "Live and learn" is just the right phrase that describes Andy Kung. He kept telling us that we have to keep trying and do things on our own, and that is the most important thing I have learned from him. Don't wait for others to tell you the answer. We have to find it by ourselves. I believe I've made the right decision three years ago to join Andy Kung's group and I'm really happy to be here working with him for these three years.

Also, I want to thank Prof. Shang-Da Yang for his kindness and great courses. Whenever we asked him about problems we met in our experiments, he always helps us find solutions with patience. Besides, I learn almost all the fundamental knowledge about ultrafast optics from him. It's really nice to have such a good teacher.

I would also like to thank Prof. Ming-Chang Chen. He gave me a lot of suggestions on my experimental setup according to his own experience. They really helped a lot.

Special thanks to Prof. Wei-Wei Hsiang and Prof. Chia-Chen Hsu, for pointing out some problems in my experiment that I have never thought about before and helping me complete my thesis paper.

I also want to thank all the colleagues in our lab. Thanks to Chih-Hsuan Lu for guiding me and being some sort of my mentor for the whole three years. Thanks to Hsiang-Nan Cheng for sharing his experience while facing problems and leading us to the championship of playing badminton. Thanks to Peggy Huang for helping us complete the HHG experiments and talking dirty jokes to make us relax while we were in pressure. Thanks to Po-Shu Wu and Yu-Chen Cheng for providing me so many useful suggestions that help me make a huge breakthrough in my experiment. Thanks to Yu-Jung Tsou, GG Chen and Ching-Che Weng for helping me with the setup and calibration of the SLM and FROG system. Thanks to Hong-Yu Chen for helping us with those LabView programs. I cannot imagine what our lab would be without you. Thanks to Pin-Hsiang Wang, Shih-Yu Yang, Hung-Wei Sun, Yi Hsun Tseng, Jen Ting Huang, Bo-Kai Hsu and Jian-Wei Lin. I really had a lot of fun with you guys during my master's years. Thanks to everyone I have met these years. It must be part of the best times in my life.

Finally, I want to thank my parents for supporting me and being proud of me all the time. Thank you for always being there for me. Without you backing me up, I couldn't have gone this far.

ABSTRACT

Supercontinuum (SC) generations have been well studied and developed in recent years. By carefully managing the dispersion, these spectrums could give us ultra-short pulses, with their pulse duration scaling down to femto-second ($1 \text{ fs} = 10^{-15} \text{ s}$) or even atto-second ($1 \text{ as} = 10^{-18} \text{ s}$) regime. There are many methods to compress a pulse such as using chirp mirrors, grating pairs, and prism pairs. As long as we have these ultra-short pulses, we can see things much clearer and observe events with more details through pump-probe experiments, generate higher order harmonics (HHG), make atto-second pulse synthesis and have many other important applications in the field of ultra-fast optics. In this thesis, we demonstrate the experiment of compressing a light source with multiple plate continuum (MPContinuum) spectrum, which was recently developed in our lab, covering almost the whole visible light range from 420 nm to 980 nm. For its programmability, we choose a spatial light modulator (SLM) as the tool to compress this pulse. With the help of two pairs of chirp mirrors, a 4-f system, and a Polarization Gating Cross-correlation Frequency Resolved Optical Gating (PG XFROG) setup, we have successfully compressed the pulse duration down to sub 3 fs.

摘要

超連續頻譜近年來已被多數實驗室所研究，藉由相位調變我們能得到在時間上脈衝寬度為飛秒等級甚至是埃秒等級的短脈衝。調變相為的方式有很多種，例如啁啾鏡、光柵對以及棱鏡對。當我們有了這樣的極短脈衝，我們便能利用它來做 pump-probe 實驗或是製造單發高階諧波脈衝以及其他很多於超快光學領域之應用。在這篇論文裡，我們利用多片熔融矽石產生從420奈米至980奈米的超連續頻譜。接著我們利用空間光調變器、兩對啁啾鏡、四焦距系統以及一個偏振態閘之交錯頻譜解析光閘系統，成功地將此光源壓縮至脈衝寬度3飛秒以下。



TABLE OF CONTENTS

Chapter 1.Introduction	7
Chapter 2.Theory	10
2.1 Fourier Optics	10
2.2 Methods of pulse compression	16
2.2.1 Prism Compressor	16
2.2.2 Grating compressor	20
2.2.3 Chirped mirrors	22
2.2.4 Self-compression	24
2.2.5 Pulse shaper	25
Chapter 3.Experiment	32
3.1 Light Source	32
3.2 Experimental Setup	34
3.2.1 4f System	36
3.2.2 Calibration	41
3.2.3 PG XFROG	47
3.2.4 Compression	50
Chapter 4.Conclusion and Discussion	61
Chapter 5.Reference	67

Chapter 1. Introduction

Laser has been invented for almost 50 years, and the scientists have been working on how to generate laser pulses with very short pulse duration, for it's an extraordinarily powerful tool to explore the world in a microscopic scale or even nanoscopic scale. These days ultra-short pulse technologies are very important and have been widely used in various fields. With the extremely short pulse width, it can provide a better time resolution for pump-probe experiments and greater microscopic resolution. Also, because of its narrow envelope width, pulses with few or less than one carrier cycle are helpful for generating higher order harmonics (HHG). As a result, people now are trying hard to push the pulse duration down to a much shorter regime.

In order to have these ultra-short pulses, we have to take good care of the spectral phase difference between different frequencies, that is, the group velocities of different colors. In recent years, ultra-short pulse compression has been achieved by several ways, and the most widely used approach is the hollow fiber compression^[1-3]. First, we focus our light source into a hollow core fiber with noble gases filled inside, the spectrum of the light source would expand to a wider range due to self phase modulation (SPM). Then, by adding some chirped mirrors right after the hollow core fiber, the pulse could be compressed down to few

femtosecond regime. This is a powerful tool because, as long as we know the spectral phase of the pulse, we can design and customize the chirp mirrors we need accordingly. The other reason for chirp mirrors to be a good choice for pulse compression is that most of them have extremely high reflectance in their designed wavelength range. This means that after passing through the whole compressing system, the pulse could still maintain its original power with just a little loss.

Pulse shaper is another promising tool. The most common pulse shaper adopted in pulse compressing experiments is the liquid crystal (LC) spatial light modulator (SLM)^[4-6]. Since it is programmable for chirp compensation, we have the ability to tune the spectral phase independently. This allows us to compress a pulse with known or even unknown phase. In addition, the phase could be controlled in a gradual way by slowly adjusting the voltage of each single pixel. The more voltage steps the SLM possesses, the more grey levels we can have. The large number of pixels a SLM have also provides us a very wide range of tunable delay, so we can compress a pulse with very large dispersion. One more advantage of using a programmable SLM is that, when it comes to ultra-short pulses with duration of just a few femtoseconds, the carrier envelope phase (CEP) becomes essential and needs to be carefully stabilized. To do so, we first need to stabilize the CEP of our Ti:Sapphire laser source, and then check if the CEP of the supercontinuum we are about to compress is also locked by using a f-2f system^[7,8]. Once we

measured the CEP of the supercontinuum, we can compensate it by adding either a constant spectral phase to shift the carrier inside the pulse or a linear spectral phase to shift the envelope of the pulse, which could be done by using the SLM.

In this thesis, the context is arranged in the following way. For chapter 2, it will be divided into two sections. In the first section, we will briefly talk about the basic concept of pulse shaping, that is, the Fourier optics. Then in the second section, we will discuss more about different types of pulse compression techniques and compare their pros and cons. For the third chapter, we will talk about the whole experiments including the light source we are compressing, the components in our system, and the algorithm we used to compress the pulse, which is assisted by Polarization Gating Cross-correlation Frequency Resolved Optical Gating (PG XFROG) measurement. The last chapter will be the discussion and the future work we are about to do.

Chapter 2. Theory

Before start compressing a pulse, we need to understand the relation between spectral phase and the pulse shape. So in chapter 2, we will first talk about Fourier optics, which describes how the frequency components would affect the pulse in time. Also, we have to know some basic concepts about phase such as group delay and instantaneous frequency. These will all be covered in section 2.1. Then in section 2.2, we will introduce some existing pulse compression techniques like chirp mirrors, grating pairs, and the SLM. We will also discuss their advantages and disadvantages. And finally we will explain why we choose a SLM to do the experiment.

2.1 Fourier Optics

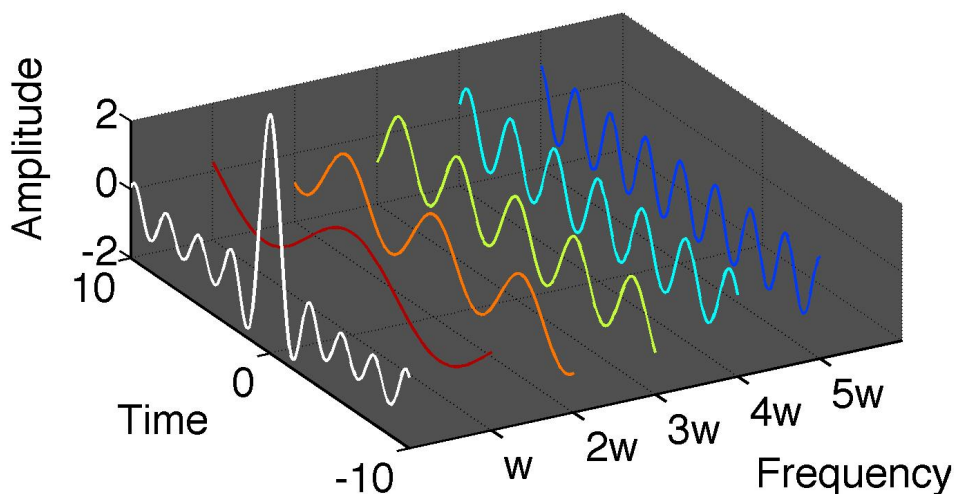


Fig. 2-1 An illustration of Fourier Synthesis with five frequency components.

According to Fourier transformation, we know that for a temporal function $f(t)$, we can find a corresponding spectrum, that is, its Fourier transformation pair :

$$F(\omega) = \int_{-\infty}^{\infty} f(t)e^{-j\omega t} dt \quad (2-1)$$

$$f(t) = \frac{1}{2\pi} \int_{-\infty}^{\infty} F(\omega)e^{j\omega t} d\omega. \quad (2-2)$$

From equation 2-2, it shows us that any temporal function $f(t)$ is composed of many different frequency components, as illustrated in Figure 2-1. The case in this figure is actually a special one because the peaks of all five frequencies are aligned together at $t = 0$. In this situation, we would say that the spectral phase is flat or is linear to frequency, and the pulse is called a transform limited (TL) pulse.

Assume we have a Gaussian shaped spectrum, we can express it in a mathematical way,

$$A(\omega) = |A(\omega)| e^{j\varphi(\omega)} \quad (2-3)$$

$$|A(\omega)| = e^{-\frac{\omega^2}{4\Gamma}} \quad (2-4)$$

$$\Gamma = \frac{(\Delta\nu \pi)^2}{2 \ln(2)} \quad (2-5)$$

$$\varphi(\omega) = \varphi_0 + \varphi_1\omega + \varphi_2\omega^2 + \dots \quad (2-6)$$

where ϖ is the frequency detuned from center frequency, $\varphi(\varpi)$ is the spectral phase and $\Delta\nu$ is the full width at half maximum (FWHM) of the Gaussian spectrum. Eq. 2-6 is the Taylor expansion of phase, and we can see that the phase could have many orders. Now if we consider only zero and first order phase,

$$\varphi(\varpi) = \varphi_0 + \varphi_1\varpi,$$

the simulated results are shown in the following figure.

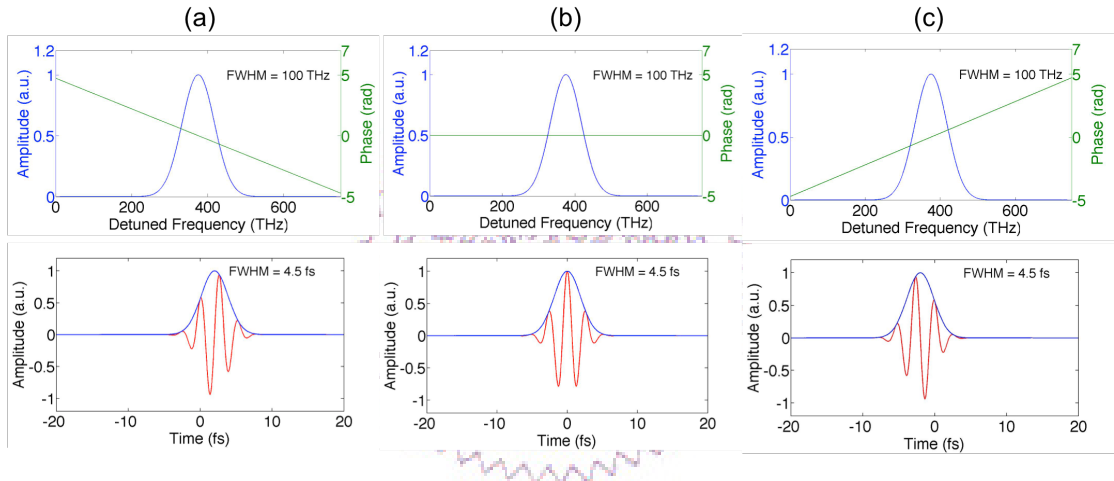


Fig. 2-2 Simulation of linear spectral phase (only first order phase) with (a) negative slope, (b) flat phase, (c) positive slope which correspond to a temporal pulse centered at (a) $t = 2$ fs, (b) $t = 0$ fs and (c) $t = -2$ fs.

Figure 2-2 is the simulation of different linear phase of a Gaussian shape spectrum centered at 375 THz with a FWHM of 100 THz. It shows that a spectrum with flat or linear phase will give us a TL pulse, except the linear phase will contribute to a shift in time domain. The pulse shape and pulse width remain unchanged. This can be explained by one of the

Fourier transform properties that for a Fourier transform pair $f(t)$ and $F(\omega)$,

$$f(t - \tau) = F(\omega)e^{-j\omega\tau}. \quad (2-7)$$

So the first derivative of the phase will result in a time delay,

$$\tau(\omega) = -\frac{d\phi(\omega)}{d\omega}. \quad (2-8)$$

This delay is called the group delay. As a result, for a linear phase, its first derivative would be its slope, that is, the group delay. Notice that the carrier inside the pulses stays still for any group delay since the zero order phases are the same for those three cases. Now if we add some second order phase, things will be a little bit different.

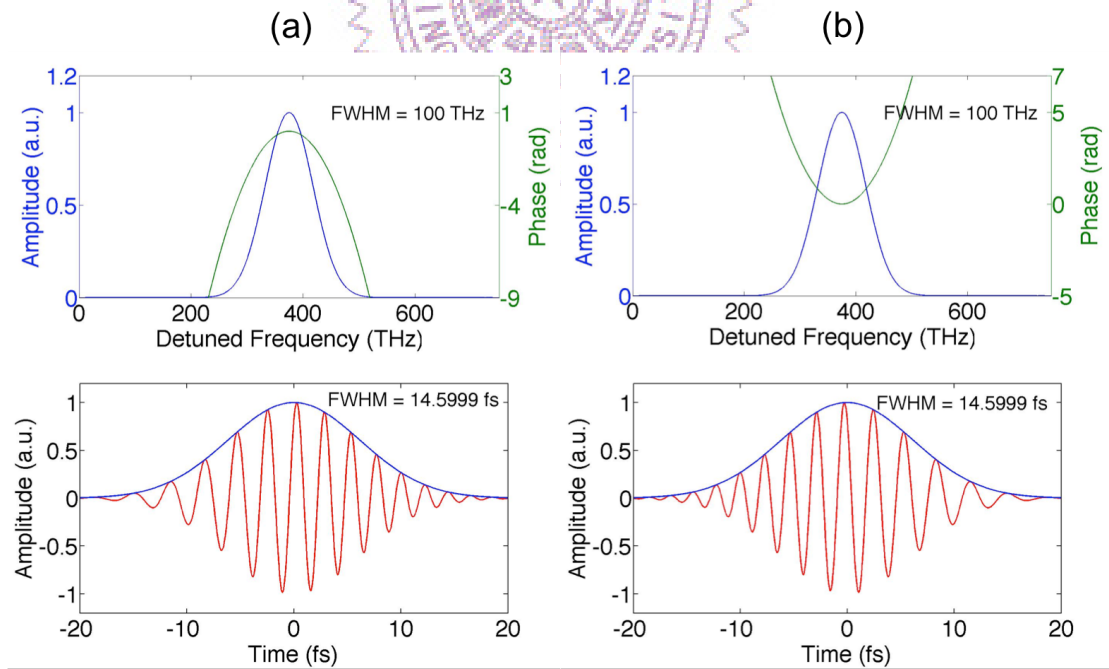


Fig. 2-3 Simulation of different second order phase with (a) negative sign, (b) positive sign.

From figure 2-3, we can see that the pulse width expand wider due to second order phase. In addition, the electric field cycles in both cases are slightly different too. For a negative second order phase, the fringe density is denser on the tailing side of the pulse than on the leading side, while a positive second order phase will lead to an opposite case. This can also be explained by equation 2-8. For a second order phase, its first derivative would be a linear function of ϖ . This means that the time delay is a function of ϖ . So different frequencies will shift away from zero point with different amount of time. The frequency at a certain time will be called the instantaneous frequency. Conventionally we often call the second order phase as “linear chirp”. The case in figure 2-3 (a) would be called “positive chirp”, “up chirp” or “normal dispersion”, and the one in figure 2-3 (b) would be called “negative chirp”, “down chirp”, or “anomalous dispersion”.

Usually, phases are induced by the materials which the pulse travels through such as air, water or glass. Any material has its own refractive index $n(\varpi)$, and the phase it induces can be written as follow,

$$\Delta\varphi(\varpi) = -n(\varpi) k L = -n(\varpi) \frac{\varpi}{c} L, \quad (2-9)$$

where $\Delta\varphi(\varpi)$ is the phase induced by material, $n(\varpi)$ is the refractive index of the material, k is the wave number and L is the distance traveled

by the pulse. The frequency dependent term is account for dispersion and can be defined as the propagation constant β that

$$n(\varpi) \frac{\varpi}{c} = \beta(\varpi), \quad (2-10)$$

and by Taylor expansion, we can express $\beta(\varpi)$ in the following way,

$$\beta(\varpi) = \beta_0 + \beta_1 \varpi + \frac{\beta_2}{2} \varpi^2 + \frac{\beta_3}{6} \varpi^3 + \dots, \quad \beta_n \equiv \frac{d^n \beta}{d \varpi^n}. \quad (2-11)$$

Again, from equation 2-8 and 2-9, we know that the group delay induced by the material is

$$\tau_g(\varpi) = -\frac{d}{d\varpi} \Delta\varphi(\varpi) = \beta_1 L + \beta_2 L \varpi + \frac{\beta_3 L}{2} \varpi^2 + \dots. \quad (2-12)$$

Now by differentiating the group delay, we can define another value called group delay dispersion (GDD),

$$D_g = \frac{d\tau_g}{d\varpi} = -\frac{d^2}{d\varpi^2} \Delta\varphi(\varpi) = \beta_2 L + (\beta_3 \varpi)L + \dots, \quad (2-13)$$

which describes how strong the chirp is induced by the dispersive medium after travelling over a distance. Since the higher order terms are usually small, we often refer to GDD as the first term $\beta_2 L$. For a positive GDD, it will result in normal dispersion, while negative GDD will give us anomalous dispersion. Sometimes we can divide the GDD by the propagation length and define it as group velocity dispersion (GVD),

$$GVD = \frac{D_g}{L} = \beta_2. \quad (2-14)$$

This value can tell us the level of chirp caused by the dispersive medium per unit length.

So far we have already introduced some basic concepts of phase and how it would affect the pulse shape in time. In the next section, we will discuss some techniques that can help us control the phase.

2.2 Methods of pulse compression

Recently, many powerful pulse compression techniques have been developed to generate ultra-short pulses. So in this section, we will cover some common ways to control the phase of a pulse such as prism compressor, grating pair, chirped mirrors and the SLM. We will also describe some details including the advantages, the disadvantages and the working principle of each method.

2.2.1 Prism Compressor

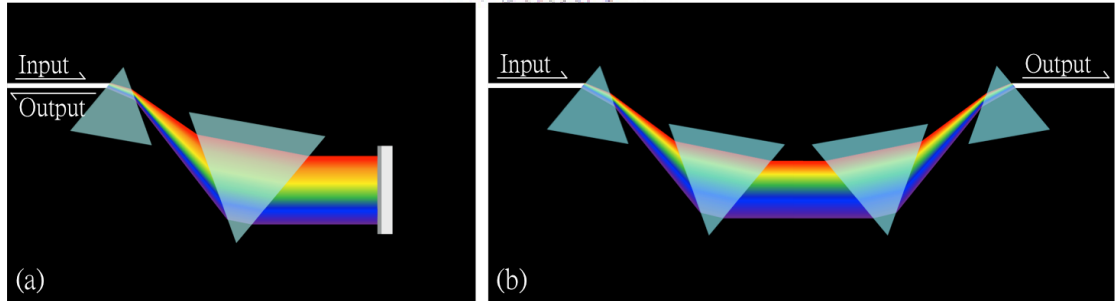


Fig. 2-4 An illustration of the setup of (a) a two-prism compressor and (b) a four-prism compressor.

Prism compressor is a very common technique to compensate unwanted dispersion. It utilizes the property that different frequencies see different refractive indices in a certain medium. For prisms made of fused

silica or BK7, lower frequencies will see smaller refractive indices, and as a consequence travel faster than higher frequencies. In this way, the prisms will provide normal dispersion if all frequencies travel same distance. So, if we wish to compensate this normal dispersion, we have to make sure that lower frequencies travel longer than higher frequencies, and this is how the prism compressors work. As shown in figure 2-4 (a), when the input pulse goes through the first prism, it will be diverted into different colors with different refraction angle according to the Snell's law. In the first prism, we can see that the blue part travels longer than the red part, which is not desired for pulse compression. To minimize this effect, we should move the input beam toward the apex of the first prism as close as possible. Also, the input beam should be incident at Brewster's angle to reduce the transmission loss. After passing through some air, the spectrally dispersed beam will enter the second prism and experience the same process, except this time the blue part travels a shorter distance than the red part in the second prism, which is good for compensating normal dispersion. Then, we can either choose a mirror to reflect the beam and form a two-prism compressor as shown in figure 2-4 (a), or add two more prisms in a symmetric way to form a four-prism compressor, as shown in figure 2-4 (b).

We can simplify this procedure and model it. Assume the center frequency travels from the first prism's apex to the second prism's apex, and the distance between the two apexes is L , as shown in figure 2-5.

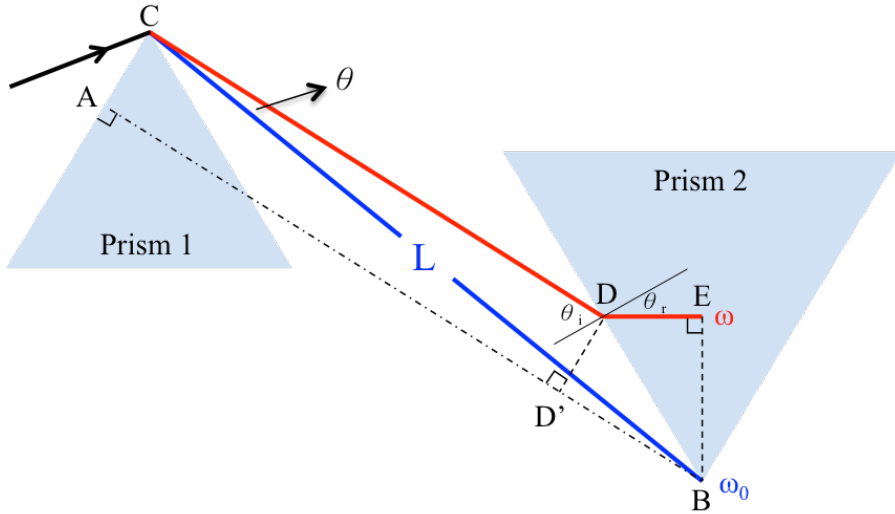


Fig. 2-5 A simplified picture of prism pair.

Now we define the angle between any diverted beam of frequency ω and the center frequency ω_0 is θ . Then we can calculate the optical path of frequency ω as follow,

$$P(\omega) = \overline{CD} + n(\omega) \times \overline{DE}. \quad (2-15)$$

Also, from Snell's law, we know that,

$$n(\omega) \sin \theta_r = \sin \theta_i. \quad (2-16)$$

Then, according to figure 2-5 and some geometric rules, we can derive that,

$$n(\omega) \times \overline{DE} = n(\omega) \times \overline{DB} \times \sin \theta_r = \overline{DB} \times \sin \theta_i = \overline{D'B} \quad (2-17)$$

$$P(\omega) = \overline{CD} + n(\omega) \overline{DE} = \overline{AD'} + \overline{D'B} = \overline{AB}. \quad (2-18)$$

By multiplying the wavenumber, we can get the effective phase. What we need to do now is to take the second and third derivative of the phase and then we can get the second order coefficient of the Taylor expansion of the phase, that is, $-\beta_2 L$, as well as the third order coefficient $-\beta_3 L$ [9],

$$\frac{\partial^2 \psi}{\partial \omega^2} = \frac{\lambda^3}{2\pi c^2} \left\{ 4L \cos\theta \left(\frac{dn}{d\lambda} \right)^2 - 2L \sin\theta \left[\frac{d^2 n}{d\lambda^2} + \left(2n - \frac{1}{n^3} \right) \left(\frac{dn}{d\lambda} \right)^2 \right] \right\} \quad (2-19)$$

$$\frac{\partial^3 \psi}{\partial \omega^3} \approx \frac{\lambda^4}{\pi^2 c^3} \left\{ 6L \cos\theta \left(\frac{dn}{d\lambda} \right)^2 - \frac{1}{2} L \sin\theta \left(\frac{d^2 n}{d\lambda^2} \right) \right\}. \quad (2-20)$$

From equation 2-19 and 2-20, we can see that it is possible for us to have both $\frac{\partial^2 \psi}{\partial \omega^2}$ and $\frac{\partial^3 \psi}{\partial \omega^3}$ larger than zero by carefully tuning the spacing between the two apex L. That is, we have the opportunity to make both β_2 and β_3 smaller than zero at the same time, and thus simultaneously compensate the second and third order dispersion. This is the advantage of using a prism compressor because normally the phase would be dominated by the second and third order.

However, there are some drawbacks of using a prism compressor. For one thing, the whole compressing mechanism relies on the refractive index, and thus is restricted by the material of the prism. For another, we will need a very large prism if we want to compress a pulse with a very broad bandwidth. Since they will divert into a larger angle, we have to

make sure the second prism is big enough so the beam will not be clipped.

2.2.2 Grating compressor

Grating compressor is another widely used technique to compress or stretch a pulse. It is commonly utilized as a stretcher in a chirped pulse amplifier (CPA) system. A basic grating compressor setup is plotted in figure 2-6.

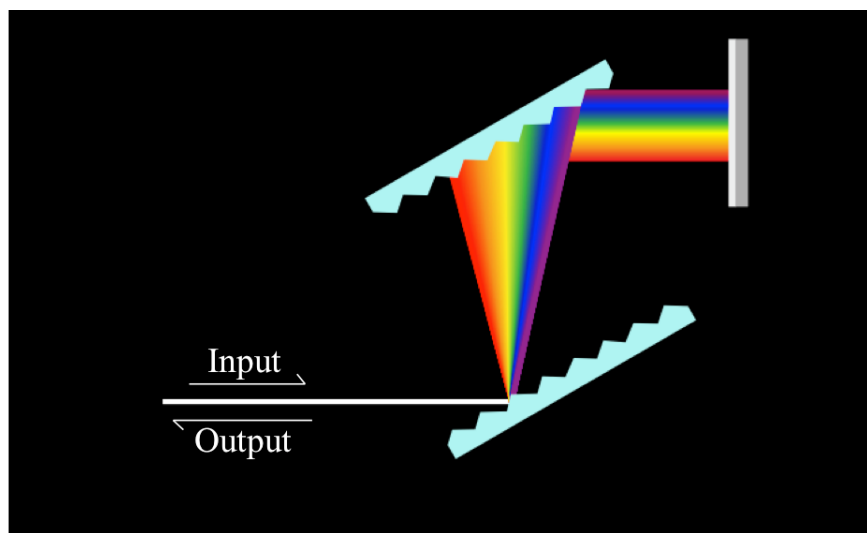


Fig. 2-6 A double-pass grating compressor.

Different from prism compressor, the compressing effect of a grating compressor depends on the number of the grooves the grating has instead of the refractive index of the material. It can also be simplified and modeled as follow.

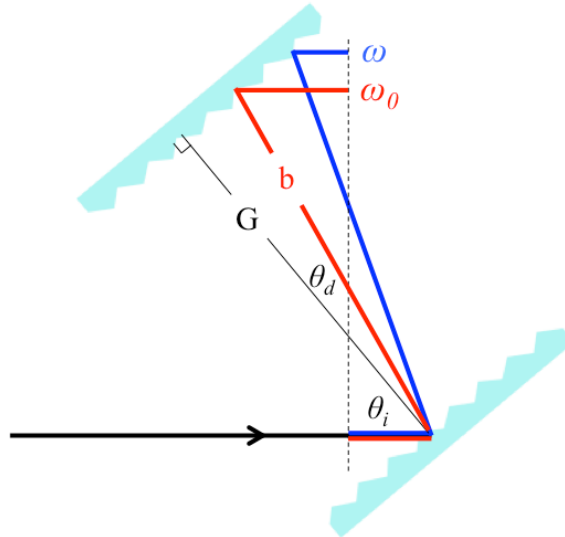


Fig. 2-7 A simplified model of a Treacy grating pair.

From grating formula and figure 2-7, we know that

$$\sin\theta_d(\omega) = \sin\theta_i + m \frac{\lambda}{d}, \quad (2-21)$$

where θ_i is the incident angle, θ_d is the refractive angle, m is the order of refraction, b is the path length of the center frequency between two gratings, λ is the wavelength corresponding to ω , and d is the space between two grooves of the grating. For $m > 0$, θ_d will be larger than θ_i , and vice versa. Similar to the analysis of prism compressor, we can calculate the optical path length of a certain frequency ω , then we can get the corresponding phase. By taking the second and third derivative, we can get the coefficients of second and third order term of the phase just as we did for prism compressor^[9],

$$\psi_2 = \frac{\partial^2 \psi}{\partial \omega^2} = \frac{m^2 \lambda^3 b}{2\pi c^2 d^2 \cos^2 \theta_d} \quad (2-21)$$

$$\psi_3 = \frac{\partial^3 \psi}{\partial \omega^3} = -\psi_2 \frac{3\lambda_0}{2\pi c} \left(1 + \frac{m\lambda_0 \sin \theta_d}{d \cos^2 \theta_d} \right). \quad (2-22)$$

From equation 2-21, we can see that ψ_2 is always larger than zero, which always introduce anomalous dispersion. We can adjust ψ_2 by tuning the spacing between two gratings. Also, the number of grooves could be well designed for desired compensation, so it is more flexible than prism compressor. But there are some trade-offs. From equation 2-22, it is clear that ψ_3 has an opposite sign of ψ_2 , which means that we can not compensate second order and third order phase at the same time. We can only optimize either second order or third order phase compensation, which is different from using a prism pair.

2.2.3 Chirped mirrors

Chirped mirror is a relatively new pulse compression tool. It is called a “chirped” mirror because it can introduce some desired dispersion simply by a few bounces between these mirrors. A general structure of the dielectric coating on the surface of chirped mirrors is shown in figure 2-8.

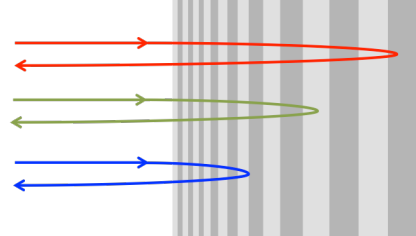


Fig. 2-8 A common structure of chirped mirrors. The bright-grey and dark-grey parts represent two materials with different refractive indices. Under this arrangement, different frequencies will see different reflectance at different depth and thus we can introduce different optical path (phase) for them after reflection.

The concept is similar to impedance matching. By carefully design the spacing and the thickness of each layer, we can control the reflectivity of different frequency components. As depicted in figure 2-8, the red part reflects deep inside the chirped mirror and as a result walks through a longer distance while the blue part reflects near the surface and thus travels a shorter path length. This will introduce negative dispersion.

Normally, this kind of design will cause some oscillation in the group delay compensation curve, like the green curve shown in figure 2-9. So usually we would design a counterpart such that the oscillation will be cancelled out as shown in figure 2-9. These two chirped mirrors are thus called double chirped mirrors (DCM) because they are always used as a pair.

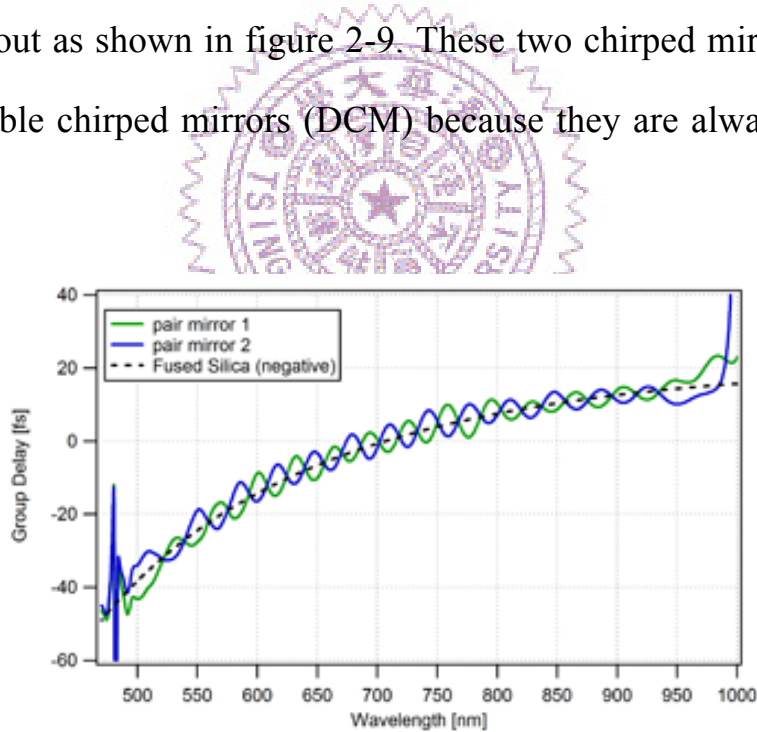


Fig. 2-9 The group delay curve of the chirped mirrors (DCM9, VENTEON) used in our experiment. It was designed to compensate the dispersion introduced by 1.2 mm Fused Silica glass.

Since we can design the chirped mirror, we can compensate almost arbitrary dispersion as long as we know the phase curve. Also, chirped mirrors usually have high reflectivity. It can help reduce the total loss if it is essential to maintain the pulse energy. But these advantages are accompanied with some disadvantages. We have to precisely characterize the pulse first. We need to know the phase difference between different frequency components that we are going to compensate to help us design the chirped mirrors. Another disadvantage is that the chirped mirrors only compensate fixed amount of phases, so we can only discretely control the phase, instead of continuously tuning it as prism compressor or grating compressor does.

2.2.4 Self-compression

Self-compression is a phenomenon that laser pulses get shorter in duration while propagating in a medium with negative dispersion. This ability has been discovered and studied for about 30 years^[10]. The most common technique is to use a photonic crystal fiber filled with noble gases^[11]. With special structure inside the fiber core, the spectrum of the pulse could be widely expanded due to self phase modulation (SPM) and meanwhile compressing itself due to the negative dispersion. Recently there's been a new tool called kagome fiber that can also generate supercontinuum and are capable of self-compressing, as shown in figure 2-10^[12].

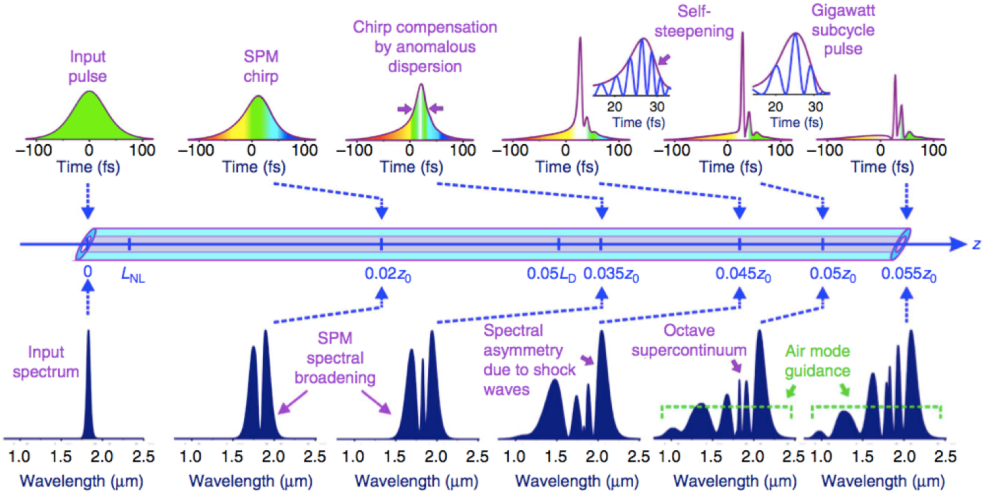


Fig. 2-10 An illustration of spectral broadening and self- compression inside a kagome fiber^[12].

Besides the PCFs, pulses inside bulk crystals can also have the ability to compress itself if its wavelength range is in the region of anomalous dispersion^[13]. These methods are more compact than the ones mentioned in previous sections since they do not need extra components such as prisms or gratings. Also, they don't need to change the direction of the path like chirped mirrors do (bounces between two mirrors). But using a fiber means that the alignment becomes critical. A little misalign may lower the coupling efficiency and cause unwanted loss at the input port. As for self-compression in bulk crystal, the output pulse energy is usually very low because of the damage threshold of the crystal.

2.2.5 Pulse shaper

Pulse Shaper is another powerful tool to compress a pulse. It is called a pulse “shaper” because we can program it by using a computer to control the phase of the pulse and thus reshape the pulse. There are two

common pulse shapers, one is called a deformable mirror, and the other one is called a spatial light modulator (SLM). In this thesis, we will only focus on the SLM because it is what we used in our experiment.

Before talking about the SLM, we have to understand the element that makes the SLM programmable, which is, the liquid crystal. Liquid crystal is a state that the molecules inside the matter aligned with each other like a crystal while they can still flow like liquid. A single liquid crystal molecule can be viewed as a uniaxial crystal, that is, it has two refractive indices n_o and n_e along two perpendicular axis, like the one shown in figure 2-10 (a). Basically, liquid crystals can be classified into three different types as shown in figure 2-10 (b), (c), and (d).

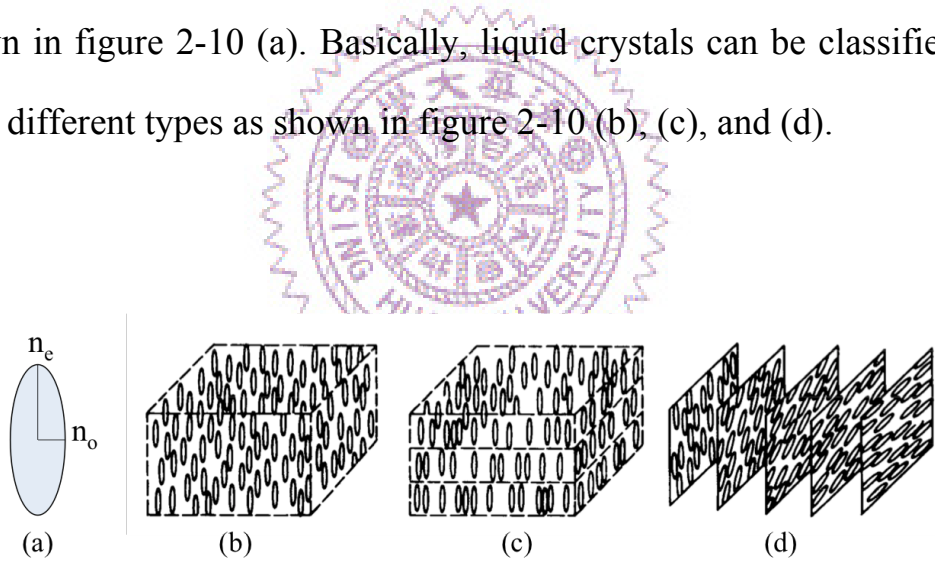


Fig. 2-11 An illustration of (a) a single liquid crystal molecule, and three different types of liquid crystal, (b) nematic, (c) smectic, (d) cholesteric.^[14]

For nematic liquid crystal, the molecules are aligned parallel to each other, but they do not stay at fixed positions. Smectic liquid crystals are similar to nematic liquid crystals since the molecules inside also tend to be parallel to each other. But their positions are not totally random. They

are grouped layer by layer, within which their positions are still random, as illustrated in figure 2-10 (b). Cholesteric liquid crystals are much different from the former two. The molecules rotate about an axis instead of standing parallel to each other.

While the molecules of a liquid crystal are aligned in certain orders, their orientation could be altered by applying external forces. For instance, when we put the nematic liquid crystals between two layers of glass plates which were rubbed at certain direction, the molecules near the plates will be forced to aligned at the same direction, as depicted in figure 2-11. This is called a twisted nematic liquid crystal. Figure 2-12 shows another way to change the molecules' direction. By applying voltage to the transparent conductive layer coated on the two glass plates, we can create an electric field. This electric field will force the liquid crystal molecules to tilt toward the field, except the ones near the two glass plates. We will discuss more in the experiment section.

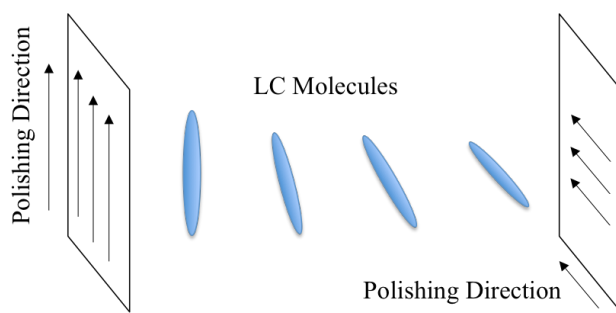


Fig. 2-12 An illustration of twisted nematic liquid crystal.^[14]

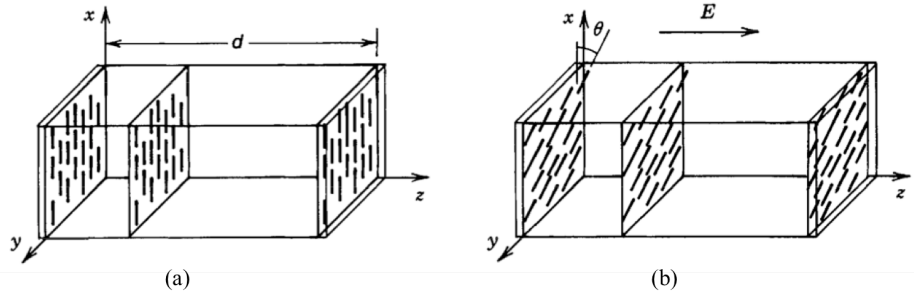


Fig. 2-13 A picture of the orientation of liquid crystal molecules (a) without, and (b) with the presence of electric field.^[14]

With this property, liquid crystals can act as wave retarder that introduces arbitrary phase or act as a wave plate that rotates the polarization of the input light by changing the applied voltage. This is how the liquid crystal spatial light modulator (LC SLM) works. Figure 2-13 shows a simplified active area of a LC SLM.

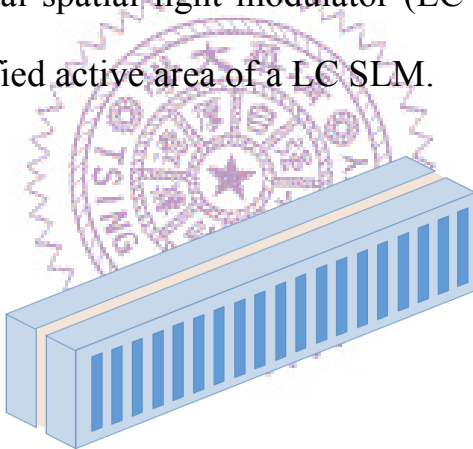


Fig. 2-14 Front view of liquid crystal part of a SLM.

As we can see, there are many pixels. Each pixel is coated with transparent conductive electrodes such as Indium Tin Oxide (ITO). This allows us to control the pixels independently. With the help of the 4f system (as shown in figure 2-14), we can distribute different wavelengths into different pixels, and thus we can control the phase of the wavelengths pixel by pixel. In this way, we can continuously compensate

almost arbitrary phases by using the SLM, which is more powerful than the methods mentioned above.

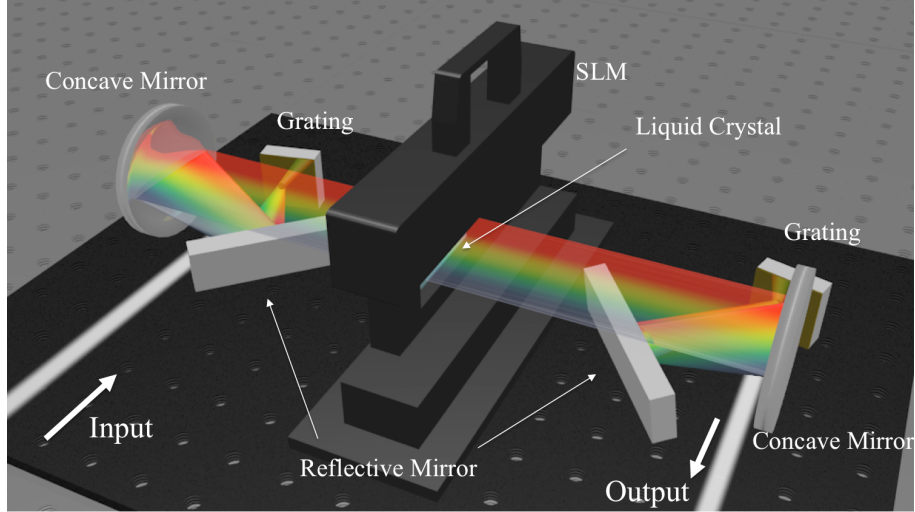
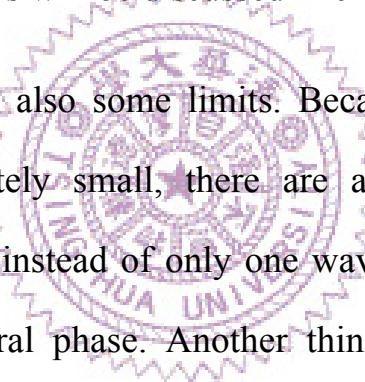


Fig. 2-15 An experimental setup of a 4f system and a LC SLM.

When compressing a pulse with the SLM, it is usually accompanied with some adaptive algorithm that tells the SLM to stop when the pulse has reached its bandwidth limit. One way to do this is to measure the second harmonic signal of the compressed pulse. Since second harmonic generation (SHG) depends on the intensity of the input pulse, as the pulse duration gets shorter during the compression process, the peak power will get much higher and as a consequence the SHG signal will be much stronger. So by slightly changing the SLM voltage pattern, we can record the SHG signal for each iteration, and the strongest one should give us the shortest pulse width. Another way is to characterize the pulse we aim to compress such as FROG or spectral phase interferometry for direct electric-field reconstruction (SPIDER). By doing so, we can have the

spectral phase information about the pulse, which can tell us how much phases we need to compensate for. This might be a better approach since we can compress the pulse and at the same time characterize it. In our experiment, we used a modified adaptive algorithm to do the job. By utilizing PG XFROG, we can measure the FROG trace. Instead of retrieving it and getting the spectral phase information, we directly use the trace as the reference to feedback to SLM. Since the PG XFROG trace is a straight line (or symmetric in shape) for a transform limited pulse^[15], our goal is to tell SLM to bend the current FROG trace to a straight line. More details will be discussed in chapter 3.2.3.



However, there are also some limits. Because the size of a single pixel cannot be infinitely small, there are a bunch of wavelengths contained in one pixel, instead of only one wavelength. This lowers the resolution of the spectral phase. Another thing is that, the maximum phase difference between two adjacent pixels is π ^[16, 17]. Then according to equation 2-12, the maximum time delay between the wavelengths of neighbor pixels is given by,

$$\tau_{g \max} = -\frac{d}{d\varpi} \Delta\varphi(\varpi) = \frac{\pi}{\Delta\varpi}, \quad (2-23)$$

where $\Delta\varpi$ is the frequency difference between two adjacent pixels. It means that if the phase change of the pulse is faster than π (strongly chirped), then this pulse cannot be compressed since the group delay

between the neighbor frequency components is too large to be compensated. The reason why the phase difference between two pixels cannot be larger than π will be discussed in chapter 4. For the SLM used in our experiment, the maximum time delay it can support for blue part (450 nm) and red part (920 nm) are estimated to be 170 fs and 694 fs, respectively.



Chapter 3. Experiment

In recent years our lab has found a new approach to generate a multi-octave spectrum in all solid medium. By simply placing a few fused silica plates together with proper spacing, we have successfully generate a broadband visible spectrum ranging from 450 nm to 980 nm at the -20dB intensity level^[18]. The beam quality of this multiple plate continuum (MPContinuum) spectrum is quite good. The relative phase of the pulse has been characterized with the help of polarization gating cross-correlation frequency resolved optical gating (PG XFROG)^[15, 19]. The beam has also been proved to be coherent both in time and in space, which indicates that this pulse is compressable. In this section, we will shortly introduce the light source we are compressing. Then we will move on to the 4f system and the SLM, including some details about the calibration of the SLM, the alignment of the setup, and the components we chose in our experiment. The method and the algorithm of adaptive pulse compression will also be mentioned in the last part, as well as the experimental results.

3.1 Light Source

The light source to be compressed in our experiment is generated by hitting multiple thin fused silica plates with a commercial Ti:Sapphire

laser with pulse width about 25 fs, repetition rate at 1 kHz, and center wavelength at 790 nm. A schematic setup is shown in figure 3-1.

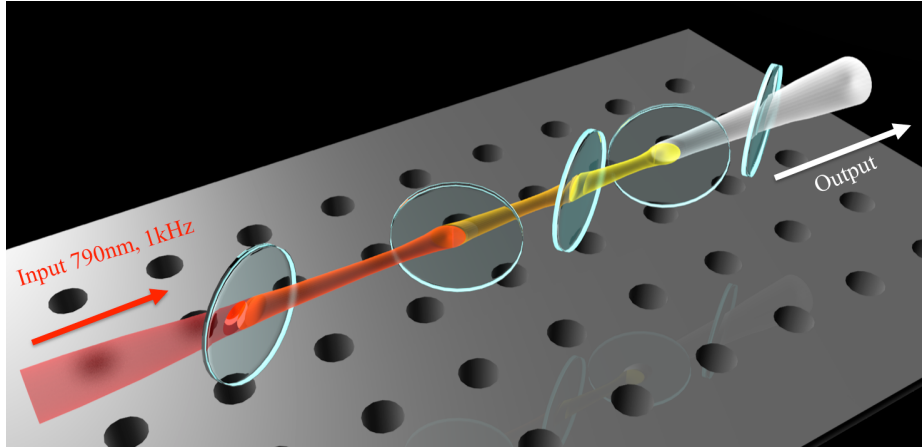


Fig. 3-1 The generation of MPContinuum with 5 pieces of $50 \mu m$ fused silica plates.

The thickness of each fused silica plate is $50 \mu m$. Different from previous work, we add a fifth plate so as to enhance the generation of shorter wavelength. The input power we used here is 250mW, and the corresponding white light spectrum can be extended from 420 nm to 980 nm at the -20 dB intensity level as shown in figure 3-2 and the average power is about 150mW.

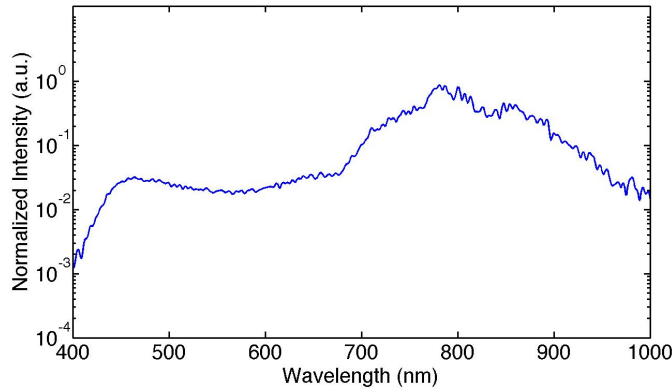


Fig. 3-2 The spectrum of MPContinuum measured by spectrometer (Ocean Optics, HR4000).

It has also been proved that the MPContinuum is not only spatially coherent but also temporally coherent. The results are shown in figure 3-3. This tells us that the phase between different frequencies are related, and thus this pulse could be compressed. So in the next section, we will talk about the experimental setup of pulse compression with the assist of a SLM.

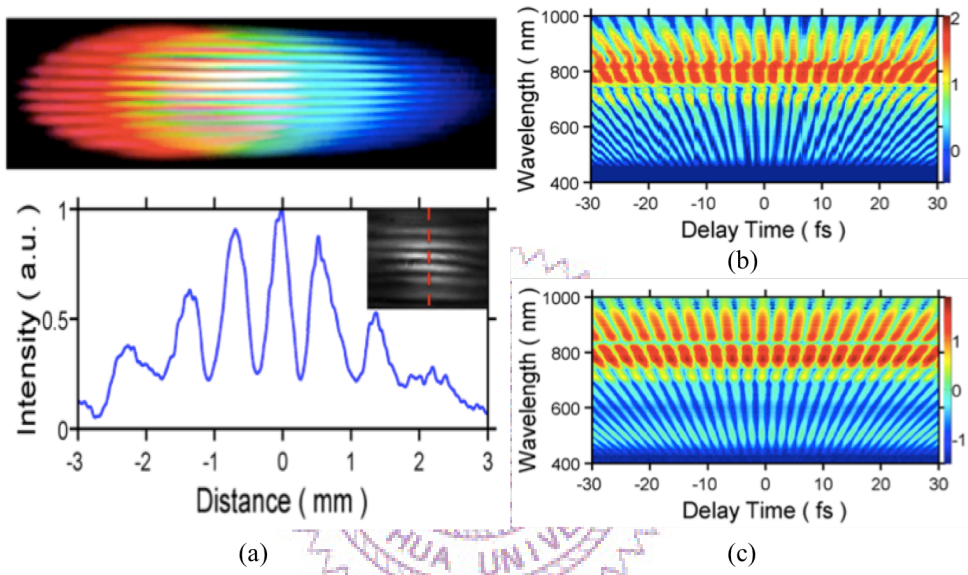


Fig. 3-3 (a) The result of a Young's interferometry. Good contrast shows the beam is spatially coherent. (b) The spectral interferometry of two sets of MPContinuum and (c) the spectral interferometry of a single set of MPContinuum. Both fringes are clear and sharp, and thus indicates that the pulse is temporally coherent.^[18]

3.2 Experimental Setup

Figure 3-4 shows the overview of our experimental setup. After passing through 5 thin fused silica plates, the central white light part is the generated MPContinuum and has an average power of 150 mW. This part is selected from the rest of the beam by an iris, and is then collimated by a silver concave mirror with radius of curvature (ROC) of 1000mm

(Thorlab). Then by using double chirped mirrors (DCM9, VENTEON), we pre-compress the pulse with 12 bounces. This is the first stage of our pulse compression system.

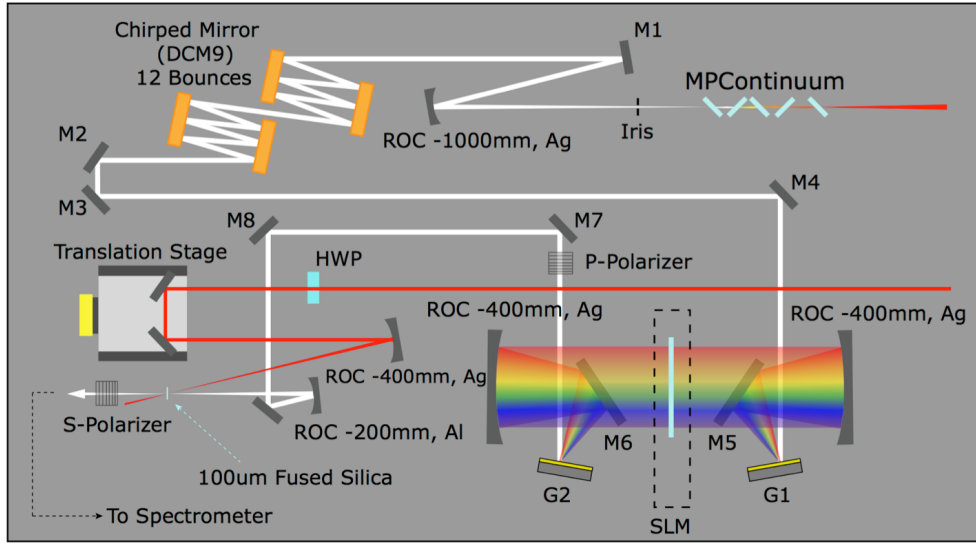


Fig. 3-4 An overall top view of the whole pulse compression setup. M1 is a silver mirror. M2~M8 are all aluminum mirrors. G1 and G2 are holographic gratings with 600 grooves/mm. P-polarizer is used due to the need of amplitude/phase modulation of the SLM. The half wave plate (HWP) and the S-polarizer are utilized in the PGX FROG system.

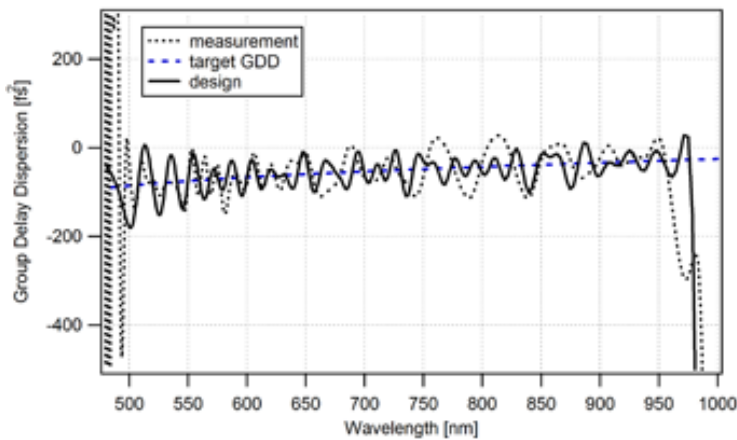


Fig. 3-5 The reflected GDD measured of DCM9 (black dotted), compared with designed data (black solid), and the compensation target (1.2mm fused silica glass, blue solid).

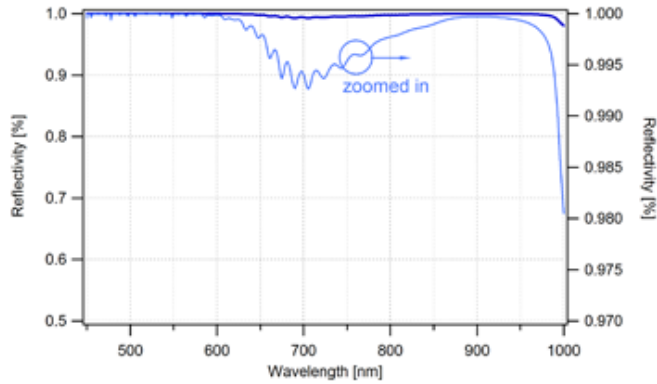


Fig. 3-6 The reflectivity of DCM9.

The specifications of the chirped mirrors are shown in figure 3-5 and figure 3-6. The high reflectivity of the chirped mirrors helps us a lot to keep our pulse energy. After a few Al reflective mirrors, the MPCcontinuum beam has the average power of about 98mW. Now we move on to the 4f system.

3.2.1 4f System

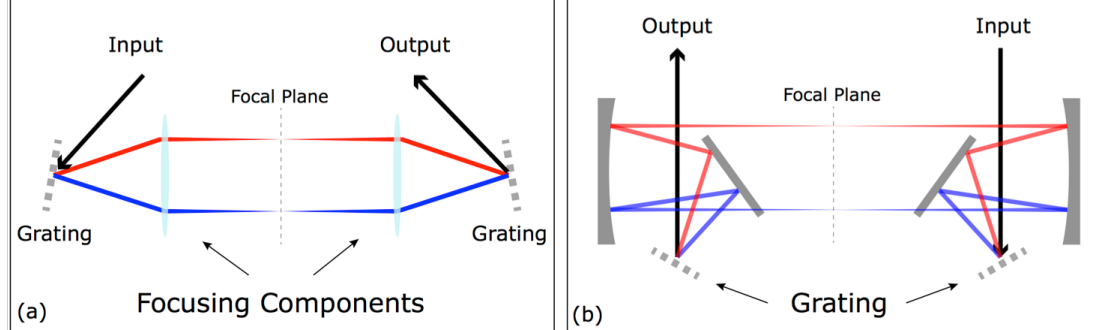


Fig. 3-7 (a) Common configuration of a 4f system. (b) The 4f system employed in our experiment.

Figure 3-7(a) shows a 4f system with two gratings and two lenses, where the “ f ” is the focal length of the lens. It is called a 4f system because the distance between the grating and the lens, and the distance between the lens and its focal plane are all equal to “ f ”. In this

configuration, we can separate the beam into different wavelength components at the focal plane, while inducing no extra phases to it. However, for the one in figure 3-7(a), the lenses will give some aberration or material dispersion if the alignment is not good enough. So in our experiment, we use concave mirrors instead of lenses, like the one in figure 3-7(b). The concave mirrors are coated with silver and the focal lengths are both 20 cm, which is the “ f ” in our 4f system. Because the width of the liquid crystal window on SLM is fixed at 6.4 cm, we need to choose a grating that can diffract the beam with a proper angle such that it can be well distributed onto the liquid crystal window with the width close to the width L of the window, as depicted in figure 3-8.

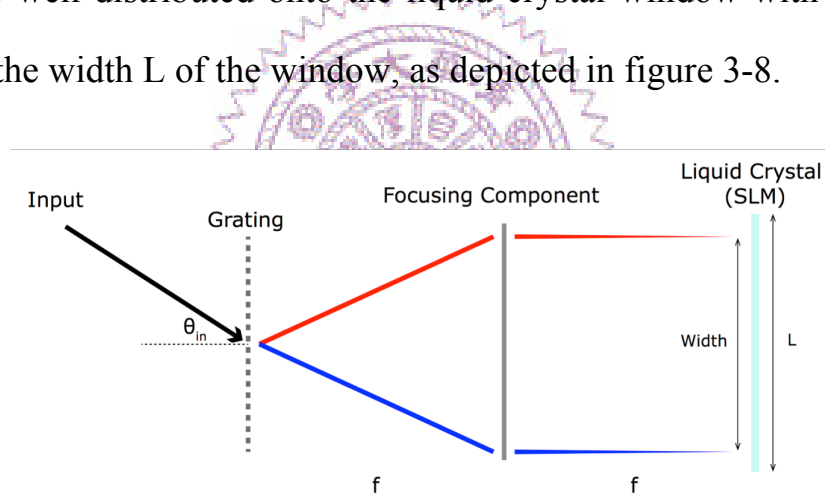


Fig. 3-8 An illustration of the design rule of a 4f system.

In our experiment, we use holographic blazed gratings (Horiba) with 600 grooves per millimeter. The spectral range is from 360 nm to 1250 nm, which covers the spectrum of our MPContinuum. Due to some concerns about the geometry of the setup, we decided to use the incident angle at around 20 degrees. Under this condition we can diverge the input beam with a diffraction angle of 19.4 degrees for the -1 order diffraction.

This will give us a spatially chirped beam with the width of 6.8cm after 20 cm. The simulated result is shown in figure 3-9. Note here that the tilt angle of the grating is very critical. We should be sure that the incident beam is or almost perpendicular to the grooves of the grating such that no extra spatial chirp is induced.

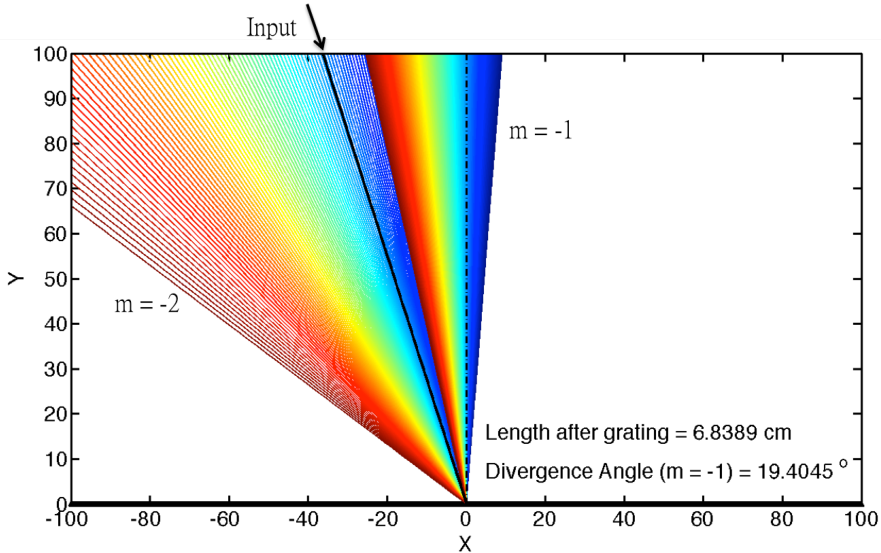


Fig. 3-9 A simulation of the diffraction of MPCContinuum with bandwidth ranging from 420 nm to 980 nm. The grating has 600 grooves/mm.

Then we put a silver concave mirror with focal length 20 cm at the first f in order to collimate the diverging beam while focusing each frequency components at another 20 cm, like the one shown in figure 3-8. Here we have to make sure that the beam is or near normal incident on the concave mirror to avoid unwanted spatial chirp and aberration. After the second f , the beam reaches its beam waist and the beam diameter is measured to be around $220 \mu\text{m}$ by a CCD camera (UCD23 Wincam). The corresponding Rayleigh range is about 8 cm to 16 cm for 920 nm and 450 nm respectively. This is the focal plane of the 4f system where we

will put our SLM. Since the thickness of the liquid crystal panel on SLM is about 6 mm, which is much thinner than the Rayleigh range, we assume that the waves here are plane waves and the beam waist will not be changed after putting on the SLM. For simplicity, we construct the other half of the 4f system in a symmetric fashion, as in figure 3-7 (b). The function of the second concave mirror is to collimate the frequency components and recombine them back into one beam. Thus the position of the second concave mirror will not only affect the dispersion of the pulse but also the beam size of the output beam. The placing of the second grating is very critical, too. Its position and tilt angle will strongly affect the beam shape and the spatial chirp of the output beam. To make sure we recombine the beam well, we focus the output beam and observe the shape at focal plane on CCD camera (Mightex). Before fine tune the grating, the shape of the focused beam was stretched as shown in figure 3-10 (a). This indicates that the beam was spatially chirped. After adjust the tilt angle of the grating, we can get a clear and almost circle-shaped beam as the one in figure 3-10 (b), which shows an almost non-spatially chirped beam.

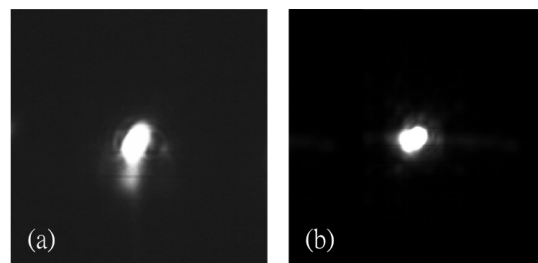


Fig. 3-10 Image of the focused output beam (a) before and (b) after adjusting the second grating in the 4f system.

Now we have completed the 4f system. We can then put the SLM in the 4f system and make sure that the liquid crystal part is at the focal plane. Because the window size is slightly smaller than the length of the diffracted beam at the focal plane, we are destined to lose some wavelength components here. Since the spectrum of MPContinuum is over an octave, some longer wavelengths of the -1 order and some shorter wavelengths of the -2 order will be overlapped. We decide to cut some infrared part off. Also, the reflectivity of silver and aluminum mirrors is relatively low at shorter wavelengths, the power of shorter wavelengths will be lost too after the 4f system. Figure 3-11 shows the spectrum of MPContinuum before entering and after leaving the 4f system as well as the SLM. The spectrum was then left from 450 nm to 920 nm. The total output average power after 4f system is measured to be 20 mW, which leads to a total transmission of the 4f system about 20%.

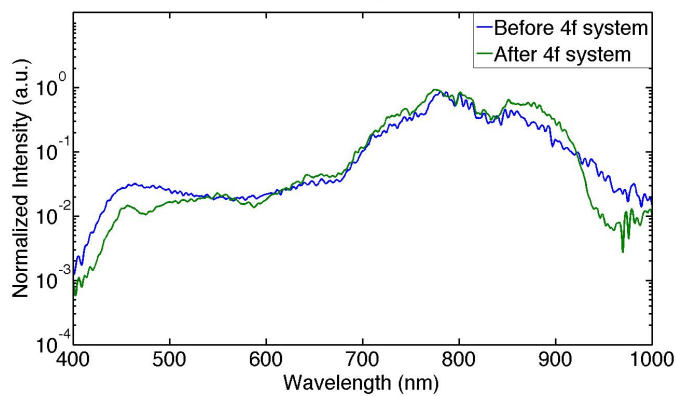


Fig. 3-11 The spectrum of the MPContinuum before and after the 4f system.

3.2.2 Calibration

Before we start compressing the pulse, we have to calibrate not only the relation between wavelengths and pixels, but also the voltage response of each pixel.

Active area	approx. 63.7 mm x 10.0 mm (SLM-S640d) approx. 31.9 mm x 13.0 mm (SLM-S320d)
Number of stripes	2 x 640/320
Stripe size	3.8 mil (96.52 μm) x 10.0/13.0 mm
Gap	0.12 mil (3.05 μm)
Liquid crystal type	nematic
Refractive index of glasses	1.53
Wavelength range	430 - 1600 nm
Transmission	>75% at 450nm – 1100nm (without polarizers, without AR coating)
Phase-/Amplitude modulation	LC director (n_e) +/-45° regarding to polarization direction maximum phase shift at 430 nm: 7π maximum phase shift at 1500 nm: 2π optional for specific wavelengths
Antireflection coating	1100 $\mu\text{J}/\text{cm}^2$ (780 nm; 250 fs; 1,85 kHz)
Damage threshold	100 $\mu\text{J}/\text{cm}^2$ (485 nm; 52 fs; 1,85 kHz) (without polarizers)

Fig. 3-12 The optical data of the SLM used in our experiment.(Jenoptik)

The SLM (SLM-S640d, JENOPTIK) we used in our experiment has two layers of liquid crystals. Each layer has 640 pixels and each pixel has a tunable voltage range of 4095 units. The optical data of the liquid crystals are given in figure 3-12, and we can see that the liquid crystal type is nematic oriented in +/- 45 degrees. Therefore each pixel of liquid crystal can act as a half wave plate with its optical axis tilted +/- 45 degrees for p-polarized input pulses. By increasing the voltage, the liquid crystal molecules will be tilted like the way shown in figure 2-12 (b), and it will equivalently change the refractive index seen by extraordinary wave (n_e). As we reaches the maximum voltage value ($V = 4095$), the molecule will be tilted almost 90 degrees and lose the function as a half wave plate. Instead, it will only act as a transparent medium with ordinary refractive

index (n_o) for all polarizations. Now if we put a p-polarizer before the 4f system and an s-polarizer after the 4f system, the beam will be blocked if it is p-polarized. In this case, we would say that the pixel is literally switched off. With this property, we can calibrate the SLM by recording the output power while changing the voltage value of the pixel.

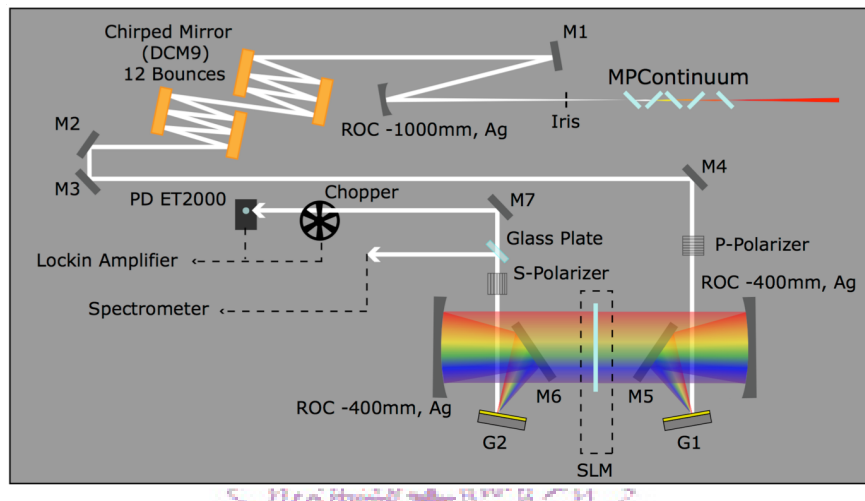


Fig. 3-13 The setup for calibration. For more details, please refer to Fig. 3-4.

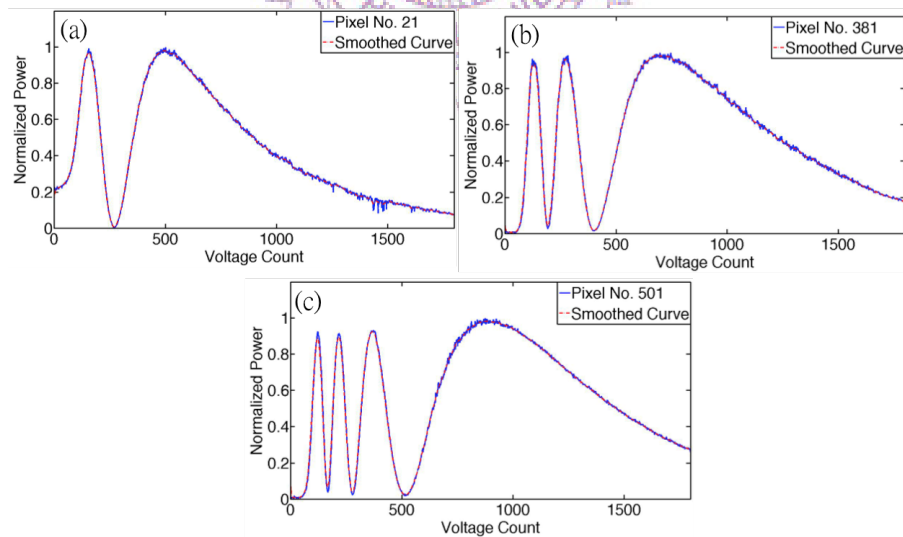


Fig. 3-14 The calibration curves of pixel (a) 21, (b) 361, and (c) 501 in layer A. The corresponding wavelengths are (a) 912.5 nm, (b) 617 nm, and (c) 517 nm. Blue curves are the measured raw data and the red curves are the smoothed curves after filtering the high frequency noises.

The setup for calibration is shown in figure 3-13. The glass plate after the s-polarizer is used to reflect some beam for recording the spectrum while turning on each pixel. It will help us determine the wavelength distribution on all pixels (see Fig 3-19(b)), and this is how we complete the position calibration. It will be described more later on. Note here that the rotation angle of s-polarizer should be well adjusted so no leakage light (projection of the polarization of the output beam onto the s-polarizer) will be detected by the spectrometer. This can help us get a better signal to noise ration (SNR) during the calibration. As for the transmitted beam, it is then sent through a chopper with frequency of 100 Hz and detected by a photo diode (PD, ET2000), which are connected to a DSP lockin amplifier (SR830). By turning off all pixels (setting the voltage to 4095), we can change the voltage of only one pixel that we wish to calibrate, and record the power detected by PD. Figure 3-14 shows three calibration curves of different pixels in layer A. Since the SLM has 2 layers and 640 pixels in each, calibrating every of them is very time-consuming. So we didn't really calibrate each single pixel for the whole voltage range. In fact, we only calibrate 31 pixels for both layer A and layer B (starting from pixel no.1, then the next one for every 20 pixels) and the voltage was only scanned from 0 to 2000. After calibrating these pixels, we can calculate the relation between phase variation and voltage change by figure 3-15 and the following formulas.

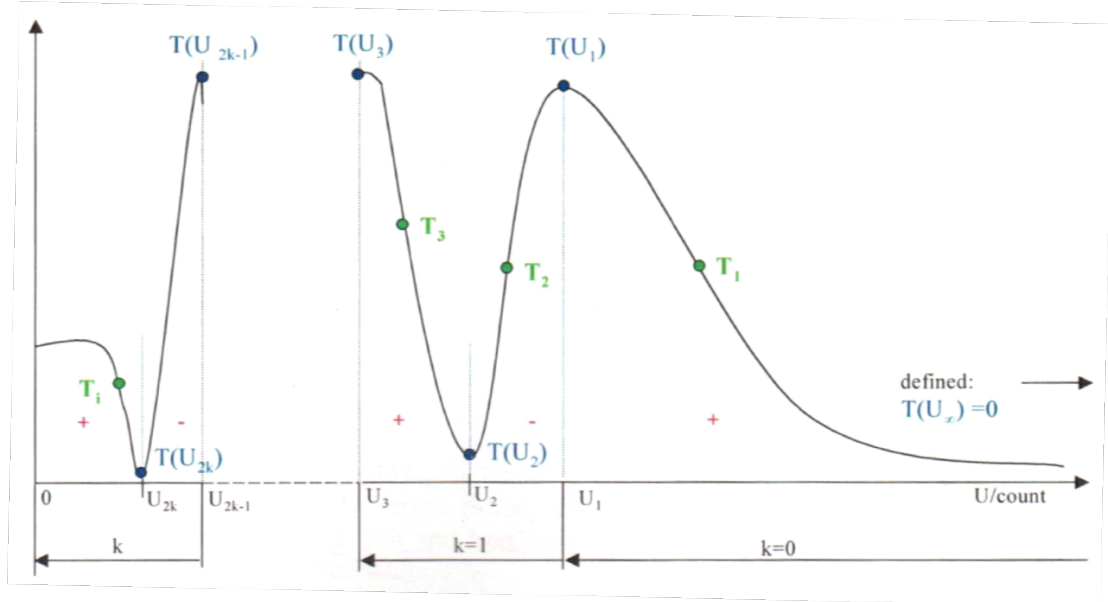


Fig. 3-15 Standardization of a measured calibration curve.

$$\left\{
 \begin{array}{ll}
 0 + 2\sin^{-1}\left(\sqrt{\frac{T(U)-0}{T(U_1)-0}}\right) & U_1 < U \\
 2\pi - 2\sin^{-1}\left(\sqrt{\frac{T(U)-T(U_2)}{T(U_1)-T(U_2)}}\right) & U_2 \leq U \leq U_1 \\
 2\pi + 2\sin^{-1}\left(\sqrt{\frac{T(U)-T(U_2)}{T(U_3)-T(U_2)}}\right) & U_3 \leq U \leq U_2 \\
 \vdots & \vdots \\
 2k\pi - 2\sin^{-1}\left(\sqrt{\frac{T(U)-T(U_{2k})}{T(U_{2k-1})-T(U_{2k})}}\right) & U_{2k} \leq U \leq U_{2k-1} \\
 2k\pi + 2\sin^{-1}\left(\sqrt{\frac{T(U)-T(U_{2k})}{T(U_{2k+1})-T(U_{2k})}}\right) & 0 \leq U \leq U_{2k}
 \end{array}
 \right. \quad (3-1)$$

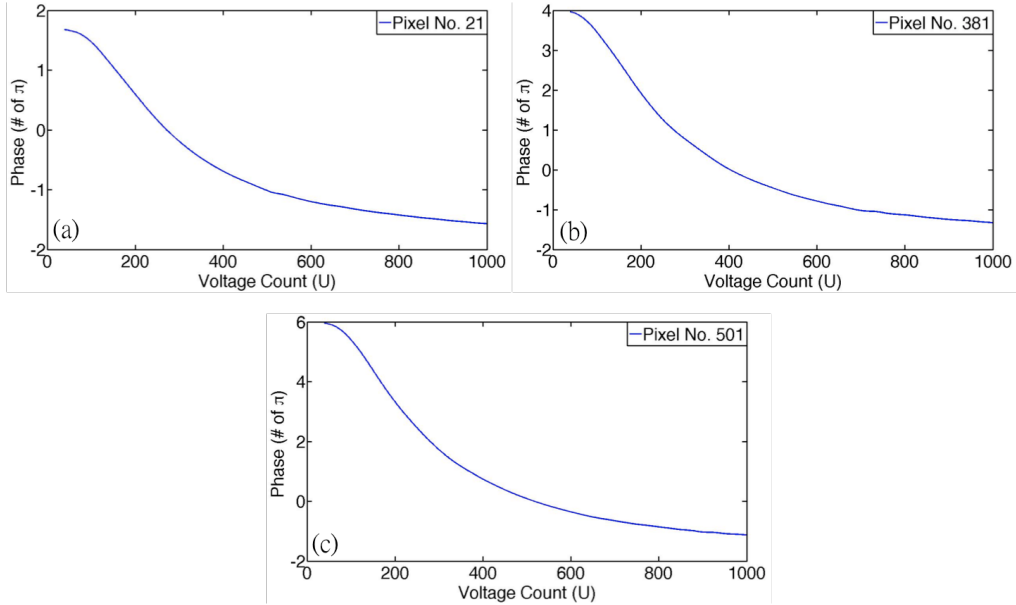


Fig. 3-16 The corresponding phase curves of pixel (a) 21, (b) 381, and (c) 501.

Once we have these phase curves, we can use interpolation to get the phase curves of the rest pixels. The whole set of measured calibration curves are shown in figure 3-17 and the interpolated phase map of layer A and layer B are presented in figure 3-18. For the following content, we will use $\Delta\phi_A$ and $\Delta\phi_B$ to denote the phase retardation of layer A and layer B, respectively.

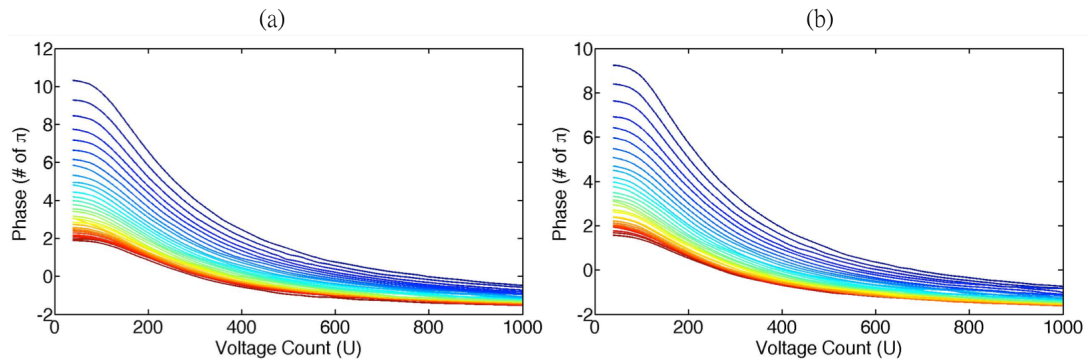


Fig. 3-17 The calculated phase curves of (a) layer A and (b) layer B. (The colors don't have special purpose. They are just for recognition.)

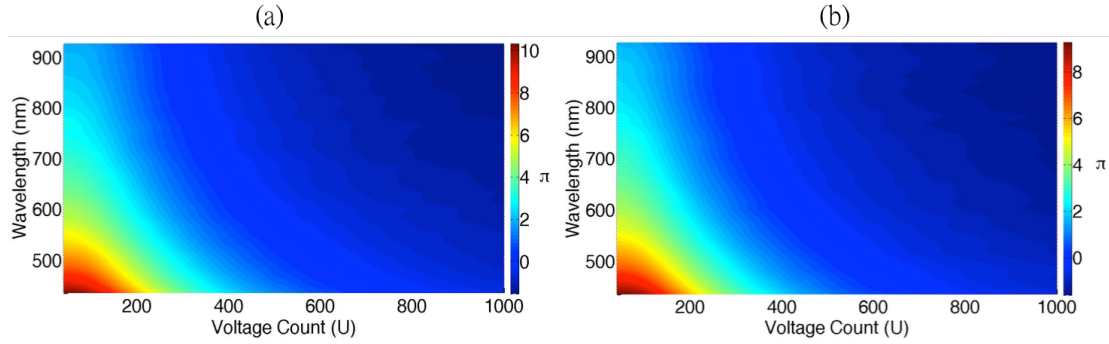


Fig. 3-18 The phase maps of (a) layer A and (b) layer B after linear interpolation.

In addition to the calibration of the phase introduced by each pixel, it is also important to calibrate the wavelength's position. Since the wavelength components are distributed in space, we need to know which component goes through which pixel, or we will just blindly tuning the phase. The distribution of wavelength components could be analyzed by the grating formula and simple geometric math as presented in figure 3-19 (a) and equation 3-2 to equation 3-4.

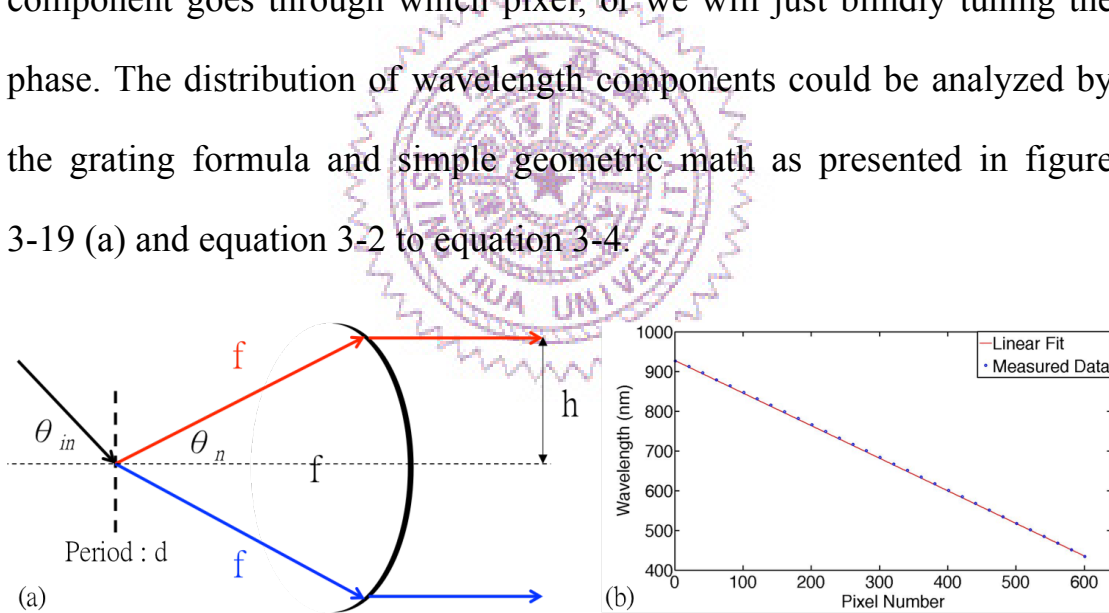


Fig. 3-19 (a) The geometry of the first f in a 4f system. (b) The measured data and linear fit of wavelength distribution on the pixels.

$$ds\sin\theta_n - ds\sin\theta_{in} = n\lambda \quad (3-2)$$

$$\theta_n = \sin^{-1}\left(\frac{n\lambda - ds\sin\theta_{in}}{d}\right) \quad (3-3)$$

$$h = f \sin \theta_n = f \left(\frac{n\lambda - d \sin \theta_{in}}{d} \right) \propto \lambda \quad (3-4)$$

By “turning on” the pixel which we want to calibrate during the calibration, we can observe the wavelength that passes through this pixel. Since the beam size is not infinitesimal, we actually see a band of wavelengths instead of only one wavelength component. In our experiment, the full width at tenth maximum (FWTM) of the wavelength range inside a single pixel is about 4 nm. Then we take the one with the highest intensity (observed from spectrometer) as the central wavelength of the pixel, and record them pixel by pixel as shown in figure 3-19(b).

As we can see, the distribution of the wavelengths on SLM is linear, just as predicted from equation 3-4.

3.2.3 PG XFROG

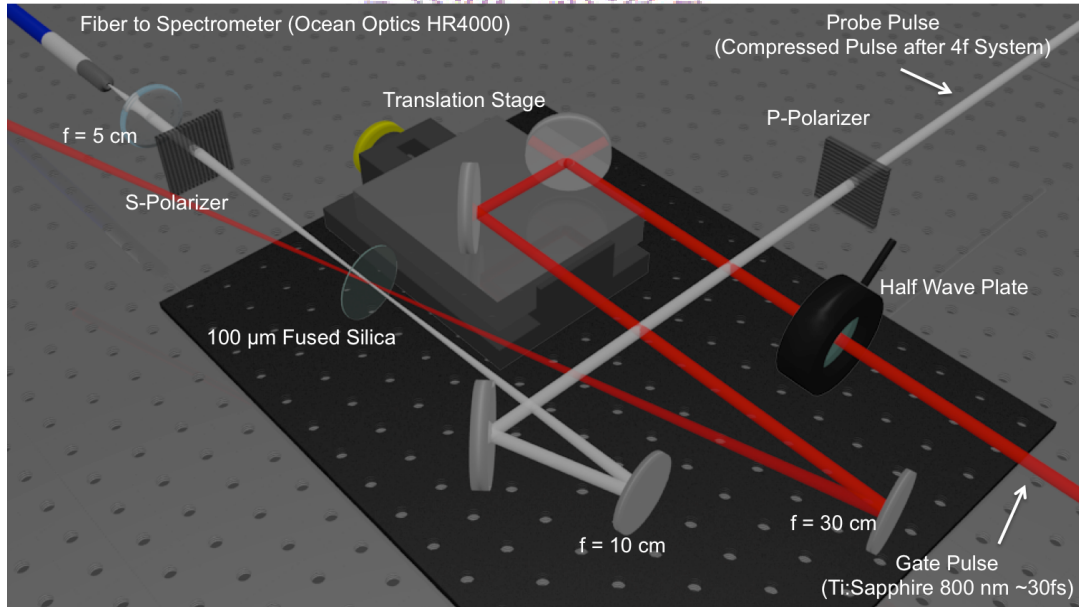


Fig. 3-20 The setup of PG XFROG after the 4f system.

As mentioned in chapter 2.2.5, if we wish to use a shaper as a tool to compress the pulse, we need to teach it how to compress, what amount of phase it needs to apply to the pulse, and when to stop the process. To do so, we need to provide the spectral phase information about the pulse so that the SLM can know how to change the voltage pattern to compensate the phase. In our experiment, we use polarization gating cross-correlation frequency resolved optical gating (PG XFROG) to characterize the pulse and measure the spectral phase. The whole setup is shown in the left-bottom corner of figure 3-4 and figure 3-20. The working principle of PG XFROG is that, for a gate pulse with linear polarization of 45° focusing onto the nonlinear medium ($100\ \mu m$ fused silica in our experiment), that point of the nonlinear medium will act as a half wave plate with the optical axis rotating 45° away from horizontal axis. That means for a p-polarized incoming pulse, it will be rotated to s-polarization after passing through that point^[15]. By placing an s-polarizer right after the nonlinear medium, we can get the PG XFROG signal, which is s-polarized and block the rest of the probe pulse. In our experiment, the half wave plate in the gate arm (red beam in figure 3-20) was used to rotate the gate pulse's polarization to 45° . The translation stage was used to create a time delay between gate pulse and probe pulse. The minimum step size used in our experiment is 100 nm, corresponding to $0.3\bar{}$ fs in time, and $0.6\bar{}$ fs for double pass configuration. Then we focused it onto the fused silica with focal length of 30 cm. For the

compressed supercontinuum pulse, it was already p-polarized after the 4f system since the phase modulation of the SLM needs a p-polarizer at the output. So we didn't add another p-polarizer for the PG XFROG. The p-polarizer shown in figure 3-20 is the same one used for phase modulation of the SLM. Then we focus it with an $f = 10$ cm concave mirror onto the point where the gate pulse was focused. The reason why we used a tighter focus for the probe pulse was because we wanted to make sure that the probe beam was fully covered by the gate beam on the fused silica. In this way, we could get the PG XFROG signal of the whole probe pulse instead of only a part of it. After the s-polarizer, we collected the PG XFROG signal with a spectrometer (Ocean Optics HR 4000).

Two things need be noted here. First, the power of gate pulse and probe pulse should not be too high, or they will induce unwanted nonlinear effect at the fused silica such as SPM to broaden the original PG XFROG spectrum, as shown in figure 3-21. To avoid this from happening, we used a glass plate and take the 4% reflection as our probe pulse and gate pulse. The average power of both is less than 1 mW.

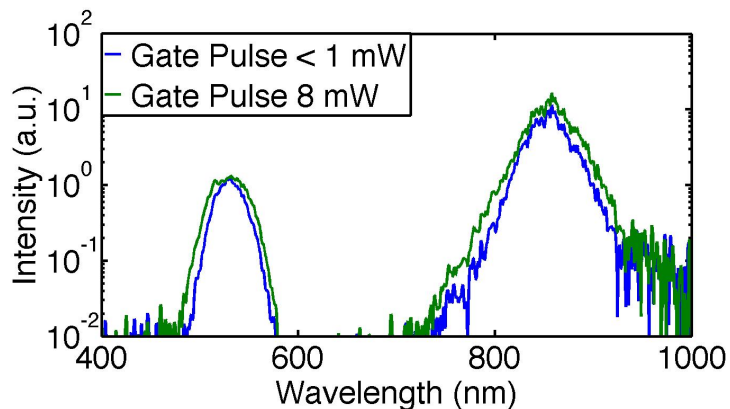


Fig. 3-21 The spectrum under some time delay between gate and probe.

Another thing is that, the cross angle between the p-polarizer at the input port of probe pulse and the s-polarizer after the fused silica should be orthogonal. If two polarizer are not perfectly orthogonal, then there would be some leakage probe beam which will also be collected by the spectrometer. The leakage probe beam will then interfere with the PG XFROG signal and cause incorrect FROG trace during the measurement.

3.2.4 Compression

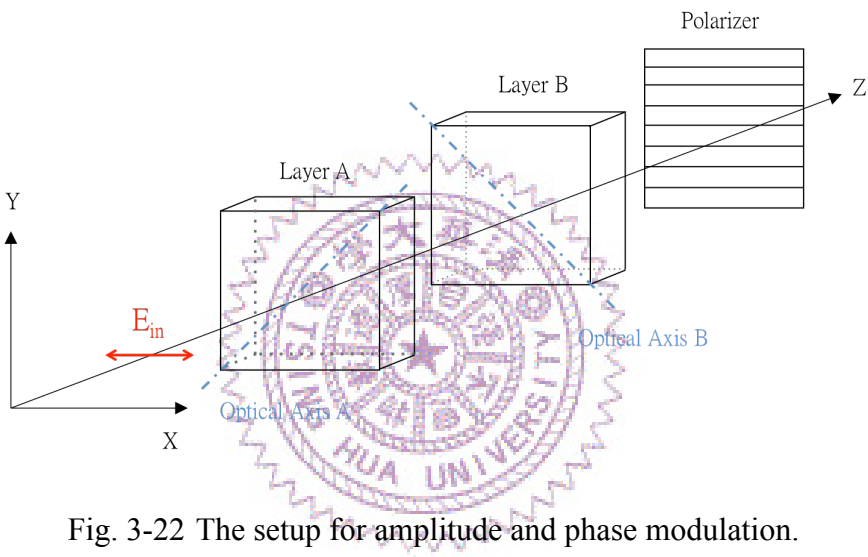


Fig. 3-22 The setup for amplitude and phase modulation.

As long as we have the phase maps, the location of the wavelengths and the PG XFROG system which can give us the spectral phase information about the pulse, we are ready to compress the pulse by modifying the spectral phase or change the shape of the pulse by modulating the amplitude of the spectrum through the SLM. The working principle could be analyzed with the help of Jones matrix. Figure 3-19 shows the setup for amplitude modulation (AM) and phase modulation (PM) of our SLM. Each component could be written as a jones matrix

and the relation between input electric field and output field is written in equation 3-5.

$$E_{out} = \begin{bmatrix} 1 & 0 \\ 0 & 1 \end{bmatrix} \cdot \begin{bmatrix} \cos\left(\frac{\pi}{4}\right) & \sin\left(\frac{\pi}{4}\right) \\ -\sin\left(\frac{\pi}{4}\right) & \cos\left(\frac{\pi}{4}\right) \end{bmatrix} \cdot \begin{bmatrix} 1 & 0 \\ 0 & e^{i\Delta\phi_B} \end{bmatrix} \cdot \begin{bmatrix} \cos\left(-\frac{\pi}{4}\right) & \sin\left(-\frac{\pi}{4}\right) \\ -\sin\left(-\frac{\pi}{4}\right) & \cos\left(-\frac{\pi}{4}\right) \end{bmatrix} \cdot \begin{bmatrix} \cos\left(-\frac{\pi}{4}\right) & \sin\left(-\frac{\pi}{4}\right) \\ -\sin\left(-\frac{\pi}{4}\right) & \cos\left(-\frac{\pi}{4}\right) \end{bmatrix} \cdot E_{in}$$

$$\begin{bmatrix} \cos\left(-\frac{\pi}{4}\right) & \sin\left(-\frac{\pi}{4}\right) \\ -\sin\left(-\frac{\pi}{4}\right) & \cos\left(-\frac{\pi}{4}\right) \end{bmatrix} \cdot \begin{bmatrix} 1 & 0 \\ 0 & e^{i\Delta\phi_A} \end{bmatrix} \cdot \begin{bmatrix} \cos\left(\frac{\pi}{4}\right) & \sin\left(\frac{\pi}{4}\right) \\ -\sin\left(\frac{\pi}{4}\right) & \cos\left(\frac{\pi}{4}\right) \end{bmatrix} \cdot E_{in}$$

↑
Phase retardation from layer A

(3-5)

For an input field polarized linearly in x-direction just as our case, the equation above could be simplified as equation 3-6.

$$\left\{ \begin{array}{l} \vec{E}_{in} = \begin{bmatrix} 1 \\ 0 \end{bmatrix} \cdot E_0 e^{j(\omega t - kz)} \\ \vec{E}_{out} = \begin{bmatrix} 1 \\ 0 \end{bmatrix} \cdot \cos\left(\frac{\Delta\phi_A - \Delta\phi_B}{2}\right) \cdot e^{j\left(\frac{\Delta\phi_A + \Delta\phi_B}{2}\right)} \cdot E_0 e^{j(\omega t - kz)} \end{array} \right. \quad (3-6)$$

Thus from equation 3-6, we realize that by controlling the phase retardation of layer A and layer B ($\Delta\phi_A$ and $\Delta\phi_B$), we can adjust the phase and amplitude of the input field.

$$\left\{ \begin{array}{l} A (AM) = \cos\left(\frac{\Delta\phi_A - \Delta\phi_B}{2}\right) \\ \phi (PM) = \frac{\Delta\phi_A + \Delta\phi_B}{2} \end{array} \right. \quad (3-7)$$

On the other hand, if we knew the phase and amplitude that we wish to apply to the field, we can also calculate the corresponding phase retardation $\Delta\phi_A$ and $\Delta\phi_B$, and thus the voltage of the pixel by looking up the phase maps.

$$\begin{cases} \Delta\phi_A = \phi + \cos^{-1}(A) \\ \Delta\phi_B = \phi - \cos^{-1}(A) \end{cases} \quad (3-8)$$

For pulse compression, we only need to deal with the phase modulation, so equation 3-8 could be further simplified to equation 3-9.

$$\Delta\phi_A = \phi = \Delta\phi_B \quad (3-9)$$

And now we can start compressing our pulse. We follow the steps described in Prof. U. Keller's textbook^[20], and the procedure is shown in figure 3-21. One thing different is that for spectral phase measurement, we used a homemade PG XFR OG system as described in previous section to reconstruct the phase information instead of using spectral phase interferometry for direct electric-field reconstruction (SPIDER).

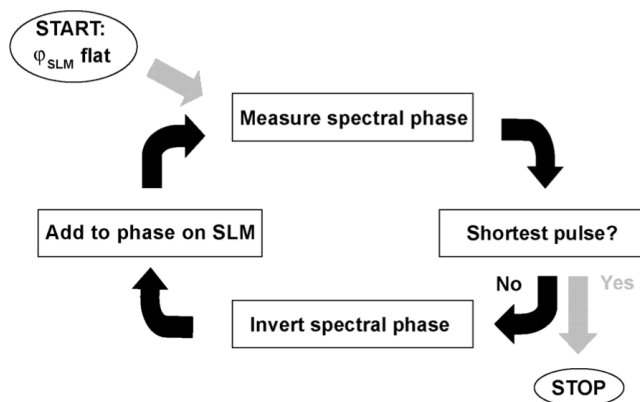


Fig. 3-23 Illustration of the steps of adaptive compression algorithm.^[20]

So first we set the voltage of all pixels on SLM to be 4095 (off), and measured the PG XFROG trace under this condition. The measured PG XFROG trace is shown in figure 3-24(a).

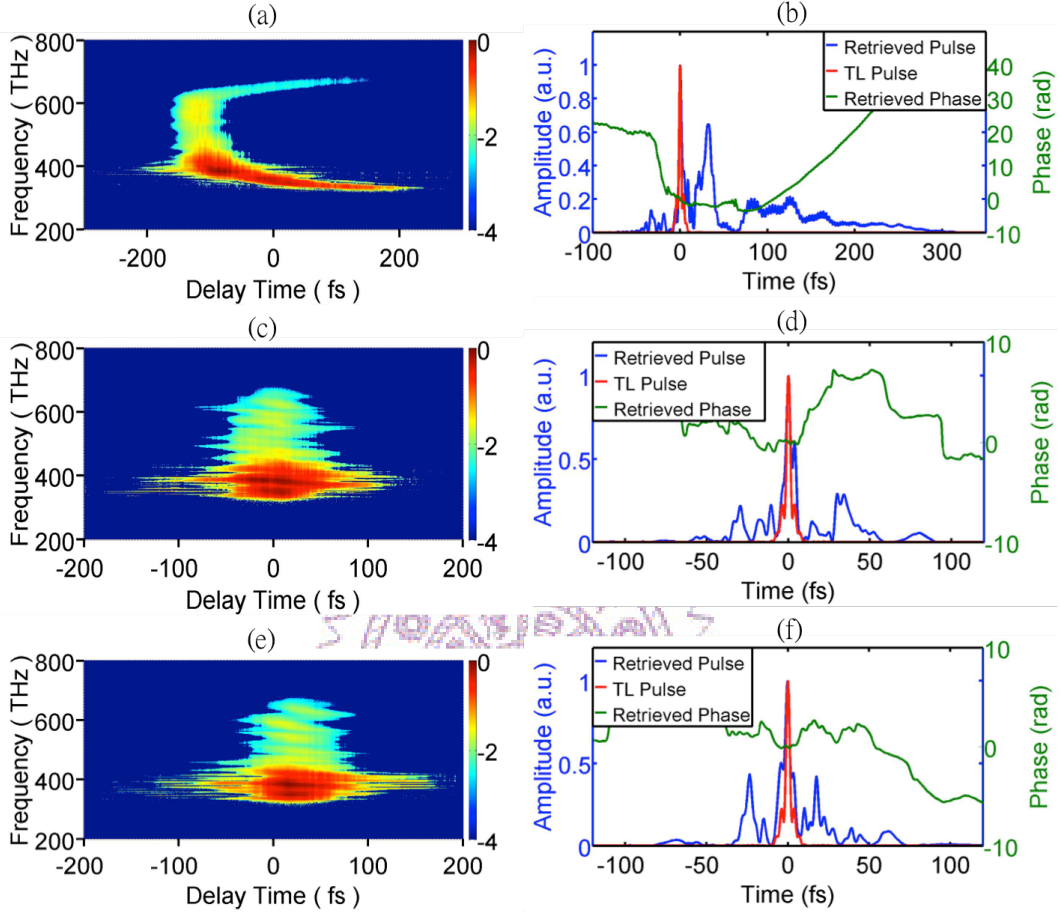


Fig. 3-24 (a) and (b) are the log scaled PG XFROG trace and retrieved time domain shape without any compensation. (c), (d) are the data after the first iteration, and (e), (f) are the data after the second iteration. The red curves in (b), (d), (f) is the transform limited pulse of full spectrum with FWHM of 2.63 fs.

Since the gate pulse was scanning through the probe pulse during the measurement, the overlap of the gate pulse and the probe pulse at arbitrary moment would tell us the spectrum it saw (or, instantaneous frequencies) at that moment. So for a transform limited pulse, we could expect the whole spectrum would appear simultaneously during the time

interval that the gate pulse overlaps with the probe pulse and then disappear when two pulses separate apart. The PG XFROG trace of a transform limited pulse should be straight-line shaped.

Apparently, the pulse is not transform limited when all pixels are set to voltage 4095, as we can see from figure 3-24(a) that the spectrum doesn't show up at the same time delay. The trace is c-shaped and some frequencies appear at different time delay. In fact, this pulse is highly chirped and the spectral phase is dominated by third and higher order phase. We can observe this from figure 3-24(a) that a group of frequencies appear at the same time (at about -100 fs in figure 3-24(a)) while the red part and the blue part show up together at other time delays. We can then intuitively imagine that the pulse shape in time domain would be a main peak followed by a long tail lasting for about 300 fs. The retrieved time domain shape confirms this idea as shown in figure 3-24(b). The quick oscillation at the tail might be caused by the interference between the red part and the blue part. After retrieving the first PG FROG result, we can get the spectral phase information. To make it a transform limited pulse, the simplest way is to add the same amount of spectral phase with a negative sign to cancel out the phase of the pulse, and this is exactly what we did in our experiment. After inverting the spectral phase retrieved from the first PG XFROG measurement, we applied it to the SLM and measured the second PG XFROG trace, which is the one in figure 3-24(c). From this figure we can

see that almost all the frequencies appear together at time 0, with some oscillations in amplitude. And the trace last from time -100 fs to 100 fs, which is smaller than the one in figure 3-24(a). This tells us that the SLM did compress the pulse. The retrieved time domain pulse shape (figure 3-24(d)) also shows that the pulse had been compressed to a smaller time interval. Following the same procedure, we made the third measurement (figure 3-24(e)) and retrieved it (figure 3-24(f)), and so on.

However, what we observed was that, each PG XFROG trace was bended back and forth near zero delay instead of being a straight line. The results were almost the same after many times of iteration. It seemed that the compressed pulse was fluctuated around the transform limited pulse for every iteration, but never had a chance to become it. The retrieved pulse shape also indicated that the pulse was not even close to a transform limited pulse. The pulse duration of each iteration can vary from 5 fs to 10 fs. This might be caused by the errors arose during the PG XFROG retrieval. Since the retrieval starts from random noises, it always results in some FROG error, which would lead to phase error that prevents getting a better compensation. Also, retrieving the measured PG XFROG trace really took a plenty of time. We had to wait for the retrieval until it reached the minimum FROG error. Sometimes it didn't even have one, meaning that we had to start over again.

To improve the adaptive compression algorithm, we adopted Yu Chen's suggestion that, since the FROG retrieval will give us undesired errors, we can directly use the PG XFROG trace as the feedback information instead of the retrieved ones. The shape of the PG XFROG trace can also provide useful information about the phase of the pulse. Because we know that the trace of a transform limited pulse is a straight line, our goal is to bend the “c-shaped” trace into a straight one. The idea of modified adaptive compression algorithm is illustrated in figure 3-25, and the details are described as follows.

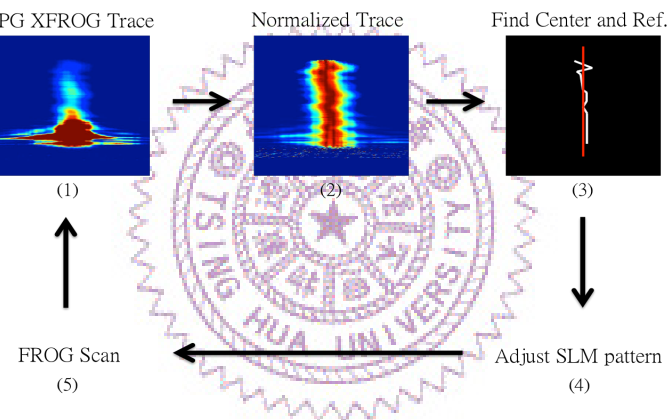


Fig. 3-25 Illustration of modified compression algorithm.

The first step of this modified adaptive algorithm is the same as before, measuring the PG XFROG trace. Then for step 2, instead of retrieving it, we normalize the peak of the trace to 1 as seen in figure 3-25 (2). The reason why we are doing so is to find the center of the trace. For each wavelength, we start scanning the intensity value of the trace from the left and also from the right. When “0.8” is found, we record the corresponding time delay. It will give us two time delays, one on the left

side of the trace and the other one on the right side, both of which correspond to the intensity value “0.8”. Then we take the average of the two time delays, and define it as the center of the trace at the wavelength. This is just like finding the full width at the 0.8 maxima of the trace, and the center would be the middle point. The reason why we pick 0.8 is because that, when measuring the PG XFR OG trace, it would fluctuate due to airflow. At some moment, some background noise would become significant, and sometimes comparable to the real signal. To avoid counting them as a part of the trace, we have to find the values that are close to the peak, that is, 1. Of course it is fine with 0.9. We just used 0.8 and found it worked well, and decided to keep using it. After calculating the center of all wavelengths, we can draw a central line of the trace (the white line in figure 3-25 (3)). Then, by calculating the average of this central line, we can draw another straight line (the red line in figure 3-25 (3)) and define it as the reference. This is the goal we wish the PG XFR OG trace of the pulse to be compressed to, and the difference between the white line and the red line is the time delay needed to be compensated by the SLM.

From equation 2-8 we know that the first integral of group delay would be the spectral phase. Thus, by integrating the difference between the central line and the reference line for each wavelength, we can get the spectral phase difference between the current pulse and the transform

limited pulse. Then we can find the corresponding voltage needed to apply to the SLM (figure 3-25 (4)). The process is shown in figure 3-26.

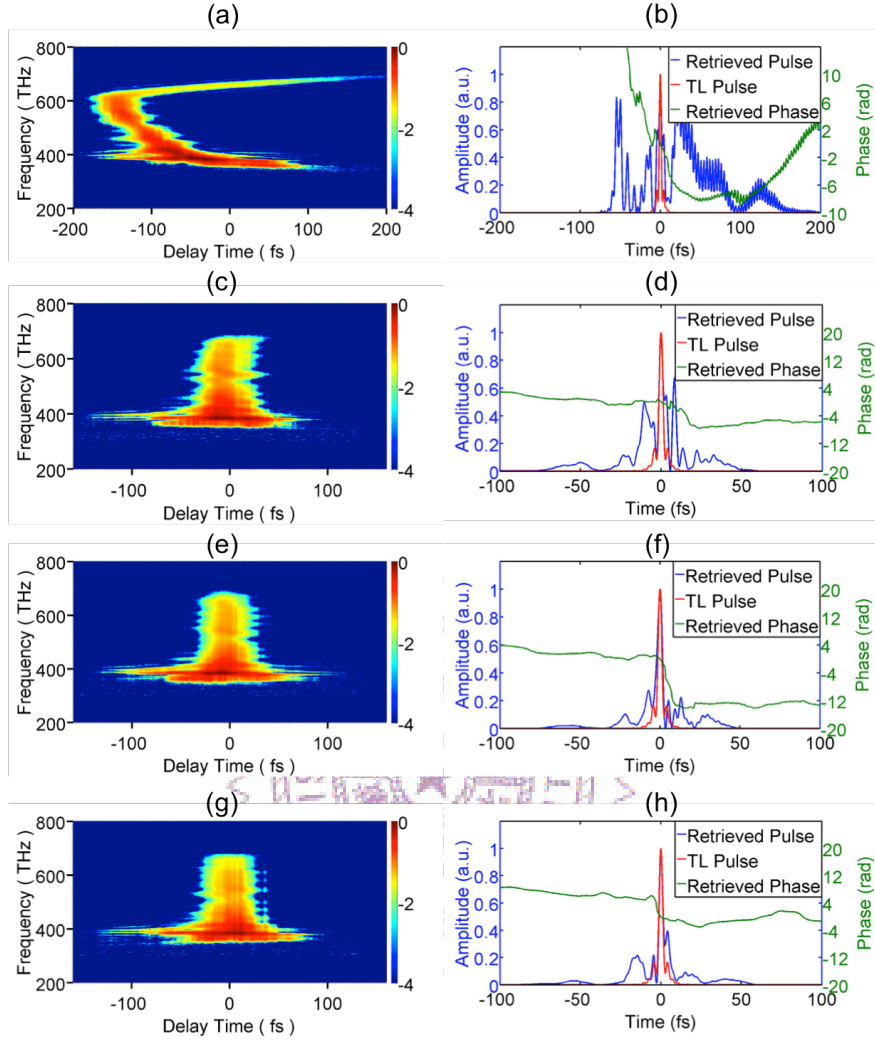


Fig. 3-26 The result of pulse compression by using modified adaptive compression algorithm. The pulse widths of the retrieved pulse in (d), (f), (h) are 11 fs, 4.3 fs and 3 fs, respectively. The transform limited pulse (red curve in (d), (f) and (h)) is estimated to have a pulse duration around 2.63fs.

By setting the initial voltage value to 4095 (off), we measure the first PG XFROG trace before any compensation, as presented in figure 3-26(a). This is slightly different from figure 3-24(a) because these two data are measured in different days, and there might be some alignment change in the setup, such as the spacing between the fused silica plates

for generating MPCcontinuum. After getting this PG XFROG trace, we followed the steps described above and made the second PG XFROG measurement. The result is shown in figure 3-26(c). We can see that the PG XFROG trace has been bended almost like a straight line, though there are still some twists inside the trace. Figure 3-26(d) also tells us that the algorithm works well since the retrieved pulse has been compressed to within 100 fs. By doing the third and the forth iteration, we can get the corresponding PG XFROG trace (figure 3-26(e), (g)) and the retrieved pulse shape (figure 3-26(f), (h)). From the PG XFROG traces, we noticed that no more twists exist inside the traces. Also, the side lobes of the retrieved pulse were getting smaller and closer to the main peak, which means that the pulse was actually being compressed toward a transform limited pulse. After few more iterations, we found that the pulse was converged to some certain degree and stop getting narrower, which is different from using the original algorithm. The best result (shortest pulse duration) occurred at the sixth iteration and the results are shown in figure 3-27, which has a retrieved pulse width of 2.78 fs.

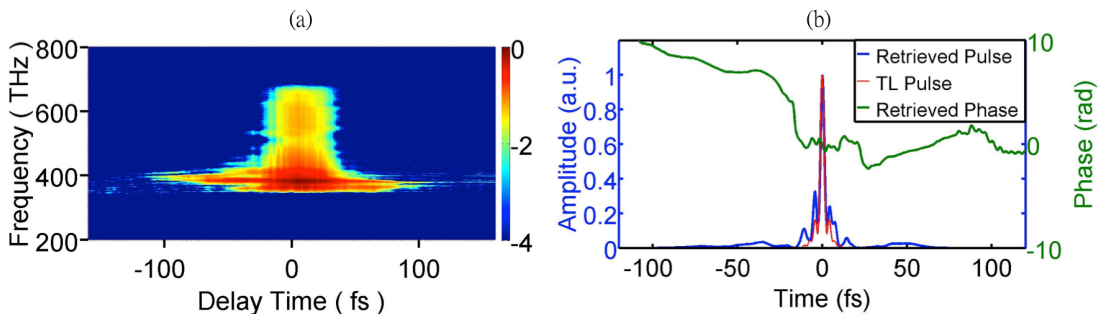


Fig. 3-27 (a) The log scaled PG XFROG trace at the 6th iteration. (b) The retrieved time domain shape with FWHM of 2.78 fs.

To summarize, we have tried two different adaptive pulse compression algorithms to compress the supercontinuum pulse generated from multiple fused silica plates. With the help of the SLM and the PG XFROG system, we are able to compress the pulse to 10 fs regime by using the original algorithm. After some modification, we use the PG XFROG trace directly as the feedback reference in our adaptive compression algorithm, and successfully compress the pulse down to sub-3 fs regime.



Chapter 4. Conclusion and Discussion

We have demonstrated a shaper assisted pulse compression technique to compress a supercontinuum with a broad bandwidth from 420 nm to 980 nm generated from multiple fused silica plates, which was reported earlier in our lab. First we used chirped mirrors to pre-compensate the pulse with 12 bounces. After that, we sent the pulse to a 4f system with a SLM, and slightly discarded some bandwidth of the spectrum during the propagation. By using the PG XFROG trace as a reference, we introduce a modified and improved adaptive algorithm for phase compensation to find the group delay we need to compensate and thus apply the correct voltage to the corresponding pixel on the SLM. Through this approach, we have successfully compressed the pulse width down to 2.78 fs, with a spectrum ranging from 450 nm to 920 nm and an average power of about 20 mW.

But still, we can see from figure 3-27 (b) that the pulse we have compressed has some residual energy left outside the main lobe. This might be caused by the imperfect calibration curves that led to improper compensation. Because the location of calibration was almost 9 meters away from the light source, the calibration curves might fluctuate due to air flow or some other environmental noises. So if we want to improve the calibration curves, we might have to move our setup closer to the

light source. Another thing is that, the 4f system in our experiment is actually not a “perfect” 4f system. We have slightly change the last “f” to induce a third order phase in order to pre compensate the pulse. This step is necessary because the SLM has its compensation limit. Since the SLM has only 640 pixels with fixed window size, the frequency difference df is then determined by the width of a single pixel. As a result, the time window of the SLM is limited and equals to the reciprocal of df , and the maximum delay provided by the SLM could not be larger than the reciprocal of $2df$. Therefore,

$$\tau_{max} = \left| \frac{d\phi}{d\omega} \right| = \frac{\Delta\phi_{max}}{\Delta\omega_{min}} = \frac{\Delta\phi_{max}}{2\pi\Delta f} \leq \frac{1}{2\Delta f} \quad (4-1)$$

$$\Delta\phi_{max} \leq \pi \quad (4-2)$$

where $\Delta\phi$ is the phase difference between two adjacent pixels and Δf is the frequency difference between the two pixels. Equation 4-2 shows that there is a limit that the spectral phase change between two pixels can not be faster than one π , or the pulse can not be compressed by the SLM, as we have mentioned in the end of chapter 2. In our case, the maximum time delay it can support is 170 fs for the blue part (450 nm) and 694 fs for the red part (920 nm).

Besides the SLM, there are also some issues in using PG XFROG measurement. First, the noninstantaneous nonlinearities of the nonlinear crystal used in PG XFROG system may lead to a broadening in pulse

duration after retrieval^[21]. Fortunately, in our system we use fused silica (SiO_2) as the nonlinear crystal, which has a relatively large bandgap that minimizes this effect^[22]. Also, the compression algorithm we use do not need to retrieve the FROG trace. We can still compress the pulse as long as the gate pulse shape has only one peak and can help us find the center of the trace. Second, the pulse width of the gate pulse ($\sim 30\text{fs}$) is much wider than the compressed pulse ($< 3\text{fs}$), so it is doubtful whether the compressed pulse duration is really below 3fs or not. So we measured the HHG spectrum to ensure it, as shown in figure 4-1.

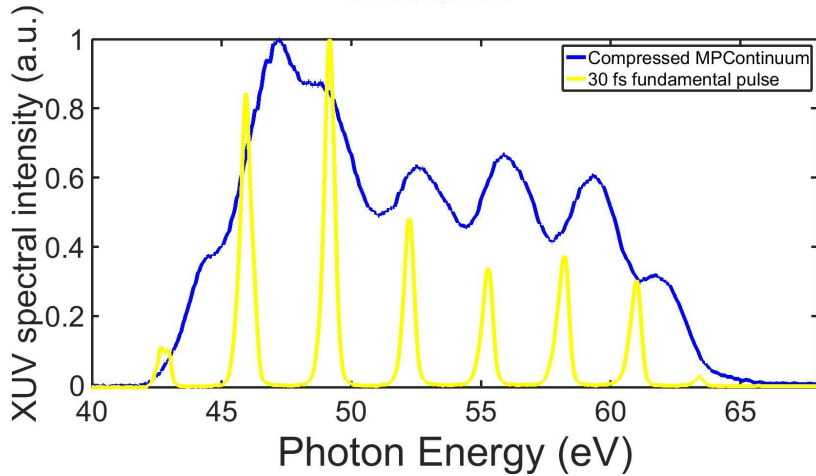


Fig. 4-1 The HHG spectrum of the compressed MPContinuum pulse (blue curve), and the fundamental pulse (yellow curve).

From figure 4-1 we can see that the HHG spectrum of MPContinuum is continuous. This indicates that the MPContinuum pulse contains near one electric field cycle inside, which equivalently gives us a pulse duration around 2.6fs.

For future works, we can divide them into three main directions, which would be (1) improvement of the light source and the compensation technique, (2) pump-probe experiments and (3) higher order harmonic isolated pulses:

(1) Light source and compression technique improvement

Since the process of compressing a pulse takes a plenty of time to finish, we should find a way to make the process much faster and more efficiently. Since the gate pulse we were using is about 30 fs, maybe we can try to use a shorter pulse as the gate pulse or just use the MPContinuum pulse to do the ordinary PG-FROG. We should need to use a second pulse measurement to confirm that the pulse is indeed being compressed to sub-3 fs such as attosecond streaking. Also, the calibration curves should be improved if we want a more precise compensation. The power of the output pulse is an important issue, too. For the following work we will try to remove the chirped mirrors and see if we can still compensate the pulse. If it works, then the average power would be expected to increase about 20%. Furthermore, if we can make sure that the spectral phase of MPContinuum is almost the same whenever we turn on the laser, then we can try to characterize it and make customized chirped mirrors to replace the current setup. Assume the reflectivity of the customized chirped of all bandwidth could be as high as 98%, then the overall average output power could be increased at least by 5 times.

(2) Pump-probe experiment

Since we compress the pulse by using a SLM, we can also modulate the amplitude of the spectrum while maintaining the phase of a compressed pulse. In this way, we can apply a cosine amplitude modulation to the spectrum and effectively create a pulse pair with identical intensity in time domain. This would be very powerful since there are no such beam splitters that can split beams with ultra-broad bandwidth. So with different cosine period, we can make the pulse pair separate with different time delay. This will allow us able to do autocorrelation experiments with very short pulses. Moreover, if we apply a cosine and a sine amplitude modulation to the spectrum, we can generate a pulse pair with different intensities whose ratio is controllable, as shown in equation 4-3.

$$F\{cos\omega\tau + r \cdot sin\omega\tau\} = (1 + r)\delta\left(t + \frac{\tau}{2}\right) + (1 - r)\delta\left(t - \frac{\tau}{2}\right) \quad (4-3)$$

By changing the ratio and the delay between the two ultra-short pulses, we can realize a pump-probe experiment that can help us observe the dynamics of atoms or even electrons.

(3) Isolated high harmonic generation (HHG)

From the semi-classical model^[23], we know that, whenever an atom is hit by an electric field, the electron will have the chance to be ionized due to tunneling effect. After that, the released electron will be accelerated by the incoming electric field. When half cycle of the field has passed, the electron will experience a force with an opposite direction that pulls the electron back during the remaining half cycle. Thus the electron will have a chance to recombine with its mother atom and release a photon of corresponding energy, which is usually in soft X ray or extreme ultra-violet (EUV). Generally, a pulse would consist of many electric field cycles if the pulse width were much longer than the field cycle. In this case, the generated HHG pulse would be a pulse train instead of a single pulse. But for a very short pulse such as sub 3 fs pulse as in our case, there is only one or one and a half cycle in each pulse. Therefore, we will have the chance to generate an isolated HHG pulse.

Chapter 5. Reference

- [1] M. Th. Hassan, A. Wirth, I. Grguraš, A. Moulet, T. T. Luu, J. Gagnon, V. Pervak, and E. Goulielmakis, “Attosecond photonics: Synthesis and control of light transients”, Review of Science Instruments **83**, 111301 (2012).
- [2] A. Wirth, M. Th. Hassan, I. Grguraš, J. Gagnon, A. Moulet, T. T. Luu, S. Pabst, R. Santra, Z. A. Alahmed, A. M. Azzeer, V. S. Yakovlev, V. Pervak, F. Krausz, E. Goulielmakis“, Synthesized Light Transient,” Science **334**, 195 (2011).
- [3] Hermance Jacqmin, Aurélie Jullien, Brigitte Mercier, Marc Hanna, Frédéric Druon, Dimitrios Papadopoulos, and Rodrigo Lopez-Martens, “Passive coherent combining of CEP-stable few-cycle pulses from a temporally divided hollow fiber compressor”, Optics Letters **40**, 5, 709 (2015).
- [4] L. Xu, *Member, IEEE*, Liming Li, N. Nakagawa, R. Morita, and M. Yamashita, “Application of a Spatial Light Modulator for Programmable Optical Pulse Compression to the Sub-6-fs Regime”, IEEE Photonics Technology Letters **12**, 11, 1540 (2000).
- [5] Keisaku Yamane, Zhigang Zhang, Kazuhiko Oka, Ryuji Morita, Akira Suguro and Mikio Yamashita, “Optical pulse compression to 3.4 fs in the monocycle region by feedback phase compensation”, Optics Letters **28**, 22, 2258 (2003).
- [6] Naoki Karasawa, Liming Li, Akira Suguro, Hidemi Shigekawa, Ryuji Morita and Mikio Yamashita, “Optical pulse compression to 5.0 fs by use of only a spatial light modulator for phase compensation”, Optical Society of America B **18**, 11, 1742 (2001).
- [7] H.R. Telle, G. Steinmeyer, A.E. Dunlop, J. Stenger, D.H. Sutter, U. Keller, “Carrier-envelope offset phase control: A novel concept for absolute optical

- frequency measurement and ultrashort pulse generation”, Applied Physics B **69**, 327–332 (1999).
- [8] Jun Ye and Steven T. Cundiff, “Femtosecond Optical Frequency Comb: Principle, Operation, and Applications”.
- [9] Andrew M. Weiner, “Ultrafast Optics”, WILEY, pp. 161-171 (2009).
- [10] L. F. Mollenauer, R. H. Stolen, and J. P. Gordon, Bell telephone laboratories, “Experimental Observation of Picosecond Pulse Narrowing and Solitons in Optical Fibers”, Physical Review Letter **45**, 13 (1980).
- [11] A. A. Amorim, M. V. Tognetti, P. Oliveira, J. L. Silva, L. M. Bernardo, F. X. Kärtner, and H. M. Crespo, “Sub-two-cycle pulses by soliton self-compression in highly nonlinear photonic crystal fibers”, Optics Letters **34**, 24, 3851 (2009).
- [12] T. Balciunas, C. Fourcade-Dutin, G. Fan, T. Witting, A.A. Voronin, A.M. Zheltikov, F. Gerome, G.G. Paulus, A. Baltuska & F. Benabid, “A strong-field driver in the single-cycle regime based on self-compression in a kagome fibre”, Nature Communications **6**, 6117 (2015).
- [13] Houkun Liang, Peter Krogen, Ross Grynko, Ondrej Novak, Chun-Lin Chang, Gregory J. Stein, Darshana Weerawarne, Bonggu Shim, Franz X. Kärtner, and Kyung-Han Hong, “Three-octave-spanning supercontinuum generation and sub-two-cycle self-compression of mid-infrared filaments in dielectrics”, Optics Letters **40**, 6 (2015).
- [14] B. E. A. Saleh, M. C. Teich, “Fundamentals of Photonics, Second Edition”.
- [15] Rick Trebino, Kenneth W. DeLong, David N. Fittinghoff, John N. Sweetser, Marco A. Krumbügel, and Bruce A. Richman et al. “Measuring ultrashort laser pulses in the time-frequency domain using frequency-resolved optical gating”, Review of Science Instrument **68**, 3277 (1997)
- [16] Andrew M. Weiner, *Senior Member, IEEE*, Daniel E. Leaird, J. S. Patel, and John R. Wullert, II, “Programmable Shaping of Femtosecond Optical Pulses by Use of 128-Element Liquid Crystal Phase Modulator”, IEEE Journal of Quantum Electronics, **28**, 4, 908 (1992).

- [17] Andrew M. Weiner, “Femtosecond pulse shaping using spatial light modulators”, Review of Scientific Instruments **71**, 5, 1929 (2000).
- [18] Chih-Hsuan Lu, Yu-Jung Tsou, Hong-Yu Chen, Bo-Han Chen, Yu-Chen Cheng, Shang-Da Yang, Ming-Chang Chen, Chia-Chen Hsu, and A. H. Kung, “Generation of intense supercontinuum in condensed media”, Optica **1**, 6, 1 (2014).
- [19] R. Weigand, J. T. Mendonca, H. M. Crespo, “Cascaded nondegenerate four-wave-mixing technique for high-power single-cycle pulse synthesis in the visible and ultraviolet ranges”, Physical Review A **79**, 063838 (2009).
- [20] Birgit Schenkel, U. Keller, M. Nisoli, J. Biegert, “supercontinuum generation and Compression”, Diss. ETH Nr. 15570, pp. 47-48 (2004).
- [21] Kenneth W. DeLong, Celso L. Ladera, and Rick Trebino, Bern Kohler and Kent R. Wilson, “Ultrashort-pulse measurement using noninstantaneous nonlinearities: Raman effects in frequency-resolved optical gating”, Optics Letters **20**, 5, (1995).
- [22] Michael Hofmann, Janne Hyyti, Simon Birkholz, Martin Bock, Susanta K. Das, Ruediger Grunwald, Mathias Hoffmann, Tamas Nagy, Ayhan Demircan, Marco Jupe, Detlev Ristau, Uwe Morgner, Carsten Bree, Michael Woerner, Thomas Elsaesser, and Guenter Steinmeyer, “Noninstantaneous polarization dynamics in dielectric media”, Optica **2**, 2, 151 (2015)
- [23] P. B. Corkum, “Plasma Perspective on Strong-Field Multiphoton Ionization”, Physical Review Letters **71**, 13, 1994 (1993).